BIOCHEMISTRY

FZD_5 is a $G\alpha_q$-coupled receptor that exhibits the functional hallmarks of prototypical GPCRs

Shane C. Wright[1,2]*, Maria Consuelo Alonso Cañizal[3,4]*, Tobias Benkel[5], Katharina Simon[5], Christian Le Gouill[2], Pierre Matricon[6], Yoon Namkung[7], Viktoria Lukasheva[2], Gabriele M. König[5], Stéphane A. Laporte[7,8], Jens Carlsson[6], Evi Kostenis[5], Michel Bouvier[2], Gunnar Schulte[1†], Carsten Hoffmann[3,4†]

Frizzleds (FZDs) are a group of seven transmembrane–spanning (7TM) receptors that belong to class F of the G protein–coupled receptor (GPCR) superfamily. FZDs bind WNT proteins to stimulate diverse signaling cascades involved in embryonic development, stem cell regulation, and adult tissue homeostasis. Frizzled 5 (FZD_5) is one of the most studied class F GPCRs that promote the functional inactivation of the β-catenin destruction complex in response to WNTs. However, whether FZDs function as prototypical GPCRs has been heavily debated and, in particular, FZD_5 has not been shown to activate heterotrimeric G proteins. Here, we show that FZD_5 exhibited a conformational change after the addition of WNT-5A, which is reminiscent of class A and class B GPCR activation. In addition, we performed several live-cell imaging and spectrometric-based approaches, such as dual-color fluorescence recovery after photobleaching (dcFRAP) and resonance energy transfer (RET)–based assays that demonstrated that FZD_5 activated $G\alpha_q$ and its downstream effectors upon stimulation with WNT-5A. Together, these findings suggest that FZD_5 is a 7TM receptor with a bona fide GPCR activation profile and suggest novel targets for drug discovery in WNT-FZD signaling.

INTRODUCTION

Frizzleds (FZDs) are ubiquitously expressed seven transmembrane–spanning receptors that interact with secreted lipoglycoproteins of the Wingless and Int-1 (WNT) family to stimulate signaling cascades involved in cellular polarization, proliferation, differentiation, and migration (*1*). On the basis of sequence homology, protein architecture, and function, FZDs have been classified as members of the class F of the heterotrimeric GTP-binding protein (G protein)–coupled receptor (GPCR) superfamily; however, their inclusion therein remains controversial. The controversy results from the scant evidence showing the functional activation of G proteins by class F receptors, a lack of motifs conserved with class A GPCRs, and a historical link with the presumably G protein–independent WNT–β-catenin pathway (*1*–*5*).

FZD_5 has been reported to interact with WNT-2, WNT-3, WNT-3A, WNT-5A, WNT-7A, WNT-7B, WNT-9B, WNT-10B, and WNT-11 in various cellular and developmental contexts, leading to numerous cellular outcomes that still require careful characterization at the molecular level (*6*–*15*). Loss-of-function studies have revealed a role for FZD_5 in ocular development, whereas gain-of-function studies have demonstrated its role in synaptogenesis (*11*, *16*). It has been demonstrated that overactive FZD_5 is responsible for the cellular proliferation of *RNF43*-mutant pancreatic adenocarcinomas (*14*). The specific combination of WNT-5A and FZD_5 has been linked to axis duplication in *Xenopus laevis*, a readout commonly associated with the WNT–β-catenin pathway (*6*, *9*, *17*). Elsewhere, it was reported that the binding of WNT-5A to FZD_5 resulted in the activation of the WNT-Ca^{2+} pathway, leading to an increase in the activity of protein kinase C (PKC) in human melanoma cells (*12*). It is not fully understood what factors promote the bifurcation of signal initiation into WNT–β-catenin and WNT-Ca^{2+} pathways.

Although the nature of FZDs as GPCRs is still poorly defined, the hallmarks that define a GPCR can reasonably be established. These include conserved agonist-promoted conformational changes, agonist-affinity changes upon G protein coupling, agonist-induced G protein subunit dissociation, and activation of specific downstream targets. Detailed insights into the structure and dynamics of receptor activation have revealed that conformational changes in helix 6 are prominent in activation of class A and class B GPCRs (*18*). This has been observed by biochemical and biophysical approaches, as well as crystal and cryo–electron microscopic structures of activated GPCRs (*19*–*24*). These structural rearrangements have also been documented by live-cell imaging–based readouts using receptor Förster resonance energy transfer (FRET) probes to monitor ligand-induced GPCR activation (*25*–*27*).

To better define the GPCR nature of FZDs, we investigated whether FZD_5 shared some of the hallmarks characteristic of prototypical GPCRs. Using live-cell imaging, spectrometric, and biophysical approaches in combination with pharmacological inhibitors, we observed that FZD_5 responds to WNT-5A with a rearrangement of intracellular loop 3 (IL3) relative to its C terminus. This movement is consistent with the functionally conserved swinging out of transmembrane domain 6 (TM6) from the receptor core, similar to class A and class B GPCRs, resulting in the engagement and activation of $G\alpha_q$. This, in turn, leads to the $G\alpha_q$-dependent production of

[1]Section of Receptor Biology and Signaling, Department of Physiology and Pharmacology, Karolinska Institutet, S17165 Stockholm, Sweden. [2]Department of Biochemistry and Molecular Medicine, Institute for Research in Immunology and Cancer, University of Montréal, Montréal, QC H3C 3J7, Canada. [3]Institute of Pharmacology and Toxicology, University of Würzburg, Versbacher Strasse 9, 97078 Würzburg, Germany. [4]Institute for Molecular Cell Biology, CMB-Center for Molecular Biomedicine, University Hospital Jena, Friedrich-Schiller University Jena, Hans-Knöll-Strasse 2, 07745 Jena, Germany. [5]Institute for Pharmaceutical Biology, University of Bonn, 53115 Bonn, Germany. [6]Science for Life Laboratory, Department of Cell and Molecular Biology, Uppsala University, P.O. Box 596, SE-751 24 Uppsala, Sweden. [7]Department of Medicine, Research Institute of the McGill University Health Center, McGill University, Montréal, QC H4A 3J1, Canada. [8]Department of Pharmacology and Therapeutics, McGill University, Montréal, QC H3G 1Y6, Canada.
*These authors share co-first authorship and contributed equally to this work.
†Corresponding author. Email: gunnar.schulte@ki.se (G.S.); carsten.hoffmann@uni-jena.de (C.H.)

diacylglycerol (DAG), the release of intracellular Ca^{2+}, and the Ca^{2+}-dependent recruitment and activation of protein kinase (PKC) at the membrane. Ultimately, these signaling events result in global cell shape changes detectable by dynamic mass redistribution (DMR). On the basis of these results, this study presents comprehensive and conclusive evidence that FZDs do indeed act as prototypical GPCRs.

RESULTS

Modeling of active FZD_5

On the basis of the hypothesis that FZD_5 acts as a GPCR, we generated structural models of mouse FZD_5 in inactive and active conformations. The inactive FZD_5 homology model was based on a crystal structure of Smoothened (SMO) in an inactive-like state [Protein Data Bank (PDB) ID: 5V56] (*28*), with which FZD_5 shares 31% identity in the entire TM region. Because the most substantial and conserved conformational change upon GPCR activation involves TM6, we modeled this helix in the active FZD_5 conformation using the G_s-bound structure of the β_2-adrenergic receptor (β_2AR) (PDB ID: 3SN6) (*20*), whereas the other regions of FZD_5 were based on the structure of inactive SMO (fig. S1, A and B). Comparison of the two FZD_5 models revealed that the conformational change of TM6 in the active state resulted in a substantial movement of the third intracellular loop (IL3) relative to the C-terminal helix 8 (Fig. 1A). On the basis of known conformational changes in class A and class B GPCRs, previously validated probes for other GPCRs (*26*, *27*, *29*, *30*), and support from the homology model of active FZD_5, we designed FZD_5-FRET probes to monitor agonist-induced conformational changes of FZD_5 by placing FRET donor and acceptor pairs in receptor domains that were predicted to undergo large movements.

Characterization of FZD_5-FRET sensors

We used mouse FZD_5 with an N-terminal V5 epitope tag to create two FRET-based biosensors (Fig. 1B). These constructs were generated by fusing cyan fluorescent protein (CFP) to the C-terminal tail of the receptor and by inserting the fluorescein arsenic hairpin binder (FlAsH)–binding motif (CCPGCC) within IL3. Placement of FRET-compatible donor-acceptor pairs in the C terminus and in IL3, respectively, has been optimized in several GPCRs to monitor the ligand-induced conformational changes associated with receptor activation in living cells (*25*). Receptor activation–associated movements affect the distance between the FRET donor (C terminus) and acceptor (IL3), resulting in changes in energy transfer. The six–amino acid FlAsH motif, which is labeled by an arsenic-containing dye, was chosen as a FRET acceptor for its relatively small size, thus limiting steric constraint in IL3. The FlAsH motif was introduced between Gly^{436} and Gly^{437} to create the sensor V5-FZD_5-FlAsH436-CFP or between the Lys^{439} and Thr^{440} for the sensor V5-FZD_5-FlAsH439-CFP (Fig. 1B). Both FZD_5 FRET constructs localized to the plasma membrane (PM) as analyzed by confocal microscopy (Fig. 1C and fig. S2A).

To evaluate the basal energy transfer between the fluorophores, we determined the FRET efficiency of the two receptor sensors by using the compound BAL (2,3-dimercapto-1-propanol) as an antidote. At high concentrations, BAL exhibits greater affinity for FlAsH than does the cysteine motif in the FlAsH-binding site inserted into the receptor (*25*, *31*). Therefore, addition of 5 mM BAL to human embryonic kidney (HEK) 293 cells expressing the different sensors scavenges FlAsH and reduces its binding to the FlAsH motif in the receptor, resulting in a dequenching of CFP fluorescence (Fig. 1D and fig. S2B). No significant difference was observed between the two sensors, which both exhibit a FRET efficiency of about 6.5% (Fig. 1E and fig. S2C). No basal intermolecular FRET was observed when V5-FZD_5-CFP was coexpressed in HEK293 cells with either V5-FZD_5-FlAsH436 (Fig. 1D) or V5-FZD_5-FlAsH439 (fig. S2B). On the basis of this validation, both V5-FZD_5-FlAsH436-CFP and V5-FZD_5-FlAsH439-CFP can serve as sensors to monitor agonist-induced intramolecular conformational changes without the confounding component of reporting on intermolecular FRET signals.

WNT-5A–induced conformational changes in FZD_5

HEK293 cells stably expressing V5-FZD_5-FlAsH436-CFP were used for further FRET experiments. Basal input of endogenously produced WNTs was reduced by preincubation overnight with LGK-974, an inhibitor of porcupine (PORCN), which is required for processing and secretion of WNTs. To investigate the conformational changes resulting from receptor activation, single cells were stimulated with saturating concentrations of purified WNT-5A, an endogenous ligand of FZD_5, using a microfluidic system that allows the delivery of a solution to one or few cells without affecting the surrounding cells (*32*, *33*). Upon WNT-5A delivery using the microfluidic device, activation of the receptor occurred 10 to 20 s after ligand addition, and the FRET ratio decreased 3 to 4% (Fig. 1F and fig. S3A). When the perfused solution was switched from ligand back to buffer, the FRET signal did not return to baseline within the time frame of the experiment (seconds), consistent with a high ligand affinity that is resistant to washout. To test the dose-response relationship between WNT-5A and the conformational rearrangements of the receptor, FRET changes were analyzed in cells stably expressing V5-FZD_5-FlAsH436-CFP (Fig. 1G) or V5-FZD_5-FlAsH439-CFP (fig. S2D) using a microplate FRET reader [half-maximal effective concentration (EC_{50}) = 677 ng/ml for V5-FZD_5-FlAsH436-CFP and EC_{50} = 765 ng/ml for V5-FZD_5-FlAsH439-CFP]. FRET signals from individual wells induced by different concentrations of the ligand were consistent with the results from the microplate reader (fig. S3B). To exclude receptor internalization as a confounding factor in the slow return to baseline after agonist stimulation, we performed bystander bioluminescence resonance energy transfer (BRET) experiments using a luciferase- and SNAP-tagged FZD_5 (SNAP-FZD_5-*R*Luc8) and either Venus-kras or Venus-Rab5 as markers of the PM and early endosomes (EEs), respectively. No changes in receptor localization, presented as the ratio of the BRET between SNAP-FZD_5-*R*Luc8 and the organelle marker Venus-kras (PM) and SNAP-FZD_5-*R*Luc8 and Venus-Rab5 (EE), were observed within a period of 20 min (fig. S3C).

FZD_5 coupling to $G\alpha_q$

On the basis of the ability of heterotrimeric G proteins to stabilize an open, active receptor conformation, we set out to address whether FZD_5 can interact with heterotrimeric G proteins. Bioinformatics analysis of the intracellular domains of FZDs predicted that FZD_5 could be a $G\alpha_{q/11}$-coupled receptor (*34*). Live-cell imaging of HEK293 cells transiently expressing V5-FZD_5-mCherry and $G\alpha_q$-Venus showed both proteins to be localized to the PM (Fig. 2A). Dual-color fluorescence recovery after photobleaching (dcFRAP) experiments using a cell membrane–impermeable chemical cross-linker to immobilize the V5-FZD_5-mCherry resulted in a decrease of the mobile fraction of $G\alpha_q$-Venus from 85.7 ± 2.1% to 72.8 ± 2.0%, indicating that the two proteins interact in living cells (Fig. 2, B to D). On the

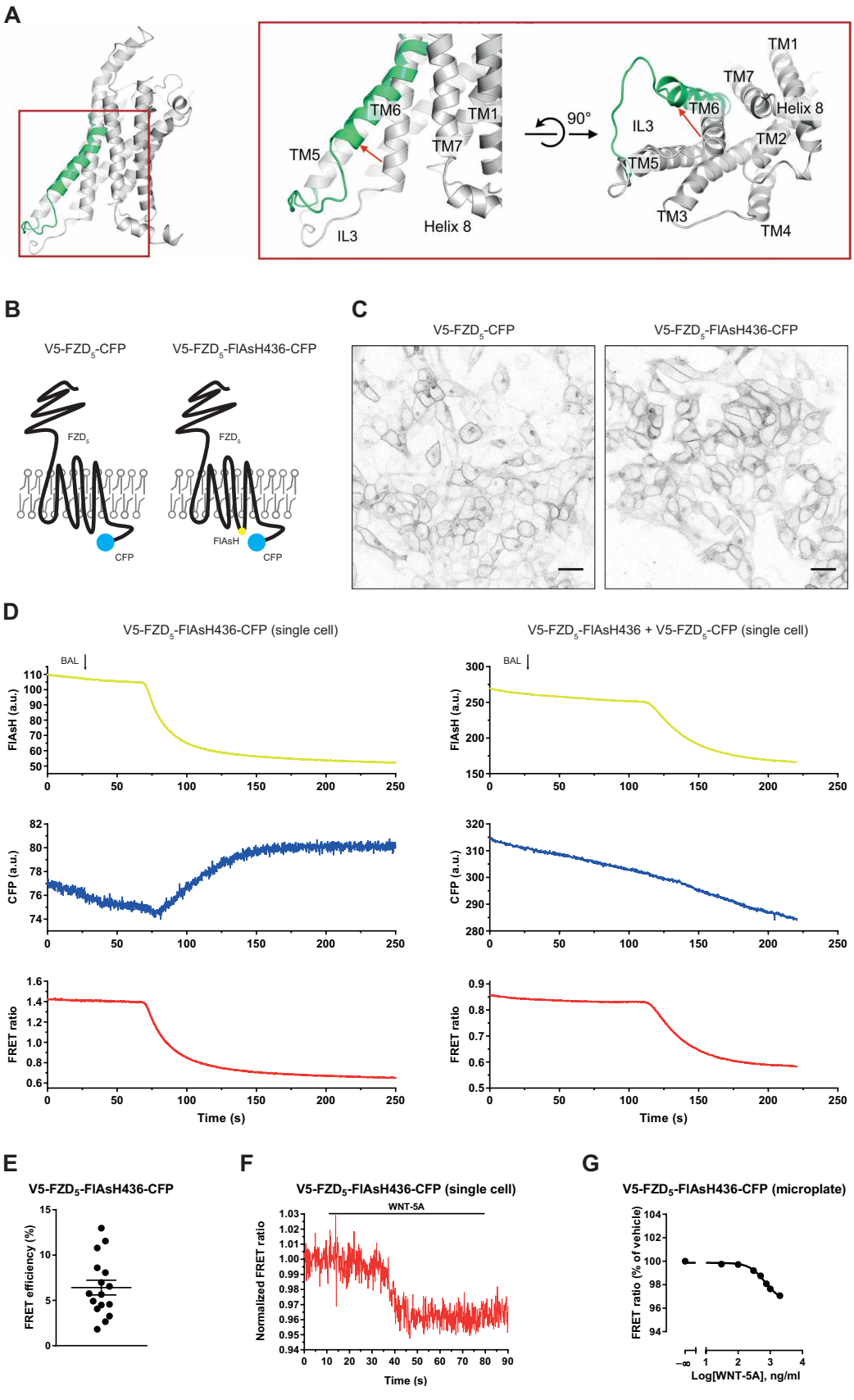

Fig. 1. Agonist-induced conformational dynamics in FZD_5 measured by FRET. (**A**) Models of FZD_5 in the active and inactive conformations. The model of the inactive conformation (gray) is based on the structure of SMO in an inactive state (PDB ID: 5V56). The model of active FZD_5 was generated using inactive SMO combined with information on the conformation of transmembrane helix 6 (TM6, green) from the G_s-bound structure of the β_2AR (PDB ID: 3SN6). The predicted movement of TM6 from the inactive to the active conformation is highlighted with a red arrow. (**B**) Illustration depicting FZD_5 constructs used in FRET experiments. All constructs were cloned with an N-terminal V5 tag into CFP N1 vectors. The black line represents unedited FZD_5 sequence. For V5-FZD_5-FlAsH436-CFP, the FlAsH-binding motif (CCPGCC) was inserted into IL3 at position 436. In the absence of a ligand, there is a basal energy transfer from CFP to FlAsH. Conformational changes in the receptor upon ligand binding alter the relative distance between FlAsH and CFP resulting in a change in FRET. (**C**) Representative confocal images showing CFP fluorescence in HEK293 cells expressing V5-FZD_5-CFP or V5-FZD_5-FlAsH436-CFP. $n = 3$ independent experiments. Scale bars, 25 μm. (**D**) FRET efficiency measurements from single cells expressing only V5-FZD_5-FlAsH436-CFP or both V5-FZD_5-FlAsH436 and V5-FZD_5-CFP. Addition of the compound BAL displaces FlAsH from its binding site. Fluorescence of liganded FlAsH is shown in yellow, CFP fluorescence in blue, and the FRET ratio (FlAsH/CFP) in red. Data are representative of $n = 3$ independent experiments. a.u., arbitrary units. (**E**) The FRET efficiency for V5-FZD_5-FlAsH436-CFP for individual cells was calculated and shown as a scatter plot. Data are represented as means ± SEM. $n = 16$ individual cells from three independent experiments. (**F**) The FRET ratio (FlAsH/CFP) from a representative cell is shown normalized to the first measured data point. Single cells were stimulated with saturating concentrations of recombinant WNT-5A approximately 10 to 15 s after beginning the recording. (**G**) FRET ratio (FlAsH/CFP) in HEK293 cells expressing V5-FZD_5-FlAsH436-CFP in a microplate format. Cells were stimulated with the indicated concentrations of recombinant WNT-5A. The FRET change induced by each concentration has been corrected for the signal obtained from vehicle-treated cells. $n = 3$ independent experiments. Data are represented as means ± SEM.

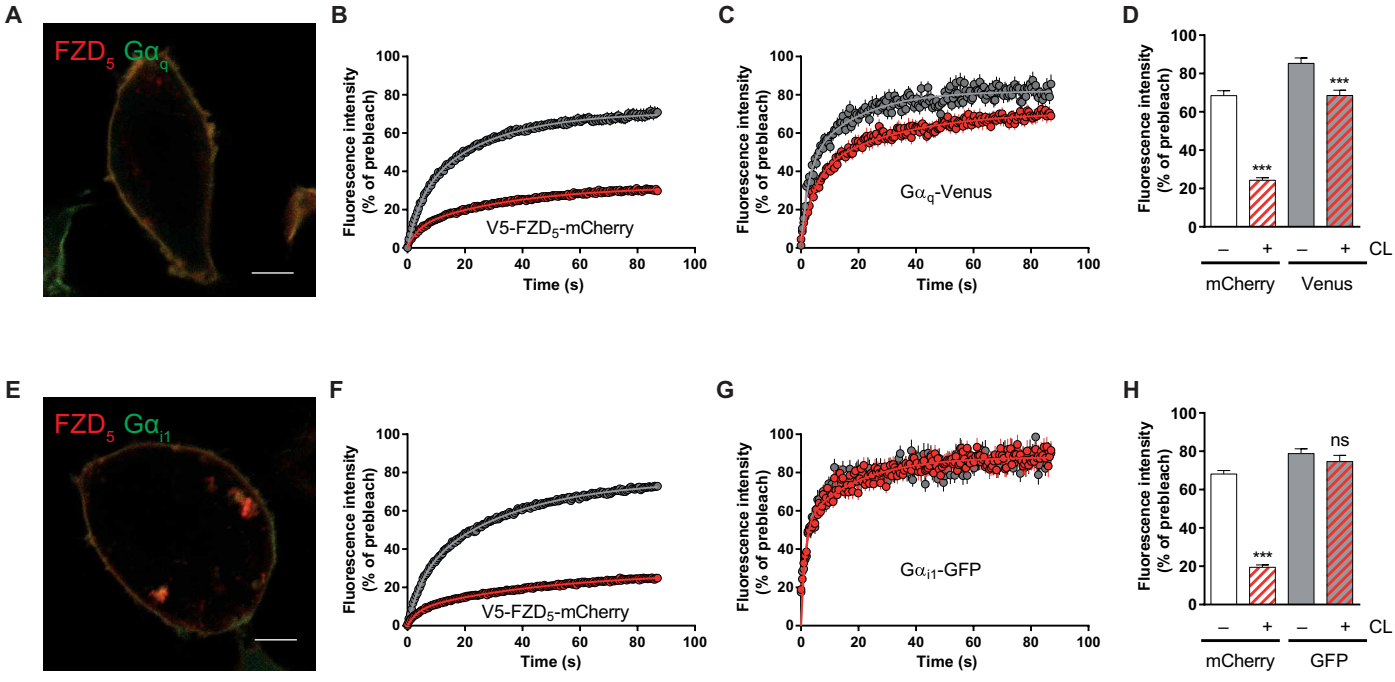

Fig. 2. FZD_5 in the inactive state forms a complex with $G\alpha_q$. (**A**) Representative image of a HEK293 cell expressing V5-FZD5-mCherry and $G\alpha_q$-Venus. These cells were used for dcFRAP experiments. Scale bar, 5 μm. (**B** and **C**) Recovery of mCherry (B) and Venus (C) fluorescence after photobleaching (FRAP) in the absence (gray) and presence (red) of surface cross-linking. The first measurement after photobleaching is time = 0. (**D**) Bar graph showing the fluorescence intensity averages of the mobile fraction of V5-FZD_5-mCherry and $G\alpha_q$-Venus before and after cross-linking (CL) within the time frame of 85 to 101 s (including 15-s prebleach measurements) as obtained by dcFRAP. White bars, V5-FZD_5-mCherry; gray bars, $G\alpha_q$-Venus; hatching, cross-linking. $n = 52$ regions of interest (ROIs) before cross-linking; $n = 66$ ROIs after cross-linking from three independent experiments. (**E**) Representative image of a HEK293 cell expressing V5-FZD_5-mCherry and $G\alpha_{i1}$-GFP. (**F** and **G**) mCherry (F) and GFP (G) FRAP in the absence (gray) and presence (red) of surface cross-linking. (**H**) Bar graph showing the fluorescence intensity averages of the mobile fraction of V5-FZD_5-mCherry and $G\alpha_{i1}$-GFP before and after cross-linking. White bars, V5-FZD_5-mCherry; gray bars, $G\alpha_{i1}$-GFP; hatching, cross-linking. $n = 41$ ROIs before cross-linking; $n = 41$ ROIs after cross-linking from three independent experiments. Data are represented as means ± SEM. ***$P < 0.0001$; ns, not significant (two-tailed t test).

basis of the previous observation that FZD_6 formed an inactive state complex with both $G\alpha_q$ and $G\alpha_{i1}$ (*35*), we hypothesized that FZD_5 would also interact with $G\alpha_{i1}$. However, and in contrast to the cross-linking experiments with $G\alpha_q$, a decrease in the mobile fraction of $G\alpha_{i1}$-GFP (green fluorescent protein) was not observed after cross-linking V5-FZD_5-mCherry (Fig. 2, E to H). These results show that, unlike FZD_6, FZD_5 selectively interacts with $G\alpha_q$, but not $G\alpha_{i1}$.

FZD_5-mediated activation of $G\alpha_q$

G protein activity biosensors are powerful molecular tools for dissecting the activation-deactivation cycles mediated by GPCRs. More specifically, the loss of resonance energy transfer (RET) between donor Gα and acceptor Gγ subunits in BRET and FRET assays is widely considered as a reliable readout for the nucleotide-dependent conformational change of heterotrimeric G proteins upon receptor activation (*36*–*38*). Their use as molecular probes for G protein activation makes them a suitable tool for confirming the existence of receptor-mediated G protein activation in living cells. First, we set out to assess the impact of WNT-induced FZD_5 activation on $G\alpha_q\beta_1\gamma_1$ complexes. WNT-5A led to a dose-dependent decrease in BRET between $G\alpha_q$-118-*R*lucII and $G\gamma_1$-GFP10 (*39*) in cells expressing SNAP-FZD_5 (EC_{50} = 51 ng/ml) (Fig. 3A), indicative of agonist-induced and FZD_5-mediated G protein activation. In cells expressing the G protein activation sensor, but not FZD_5, WNT-5A–induced changes were below the detection threshold. Consistent with the lack of change in the mobile fraction of $G\alpha_{i1}$ observed above in dcFRAP experiments, the addition of WNT-5A to cells expressing SNAP-FZD_5 did not affect the efficacy or potency of changes in BRET between $G\alpha_{i1}$-91-*R*lucII and $G\gamma_2$-GFP10—a biosensor that is readily activated by G_i-coupled receptors (*36*)—relative to endogenous FZDs (Fig. 3B).

To further evaluate the activation of $G\alpha_q$ by FZD_5 in real time, we used a previously described FRET sensor composed of $G\alpha_q$-127-mTqΔ6 + cpVenus-$G\gamma_2$ that monitors the agonist-induced and receptor-mediated activation of G_q proteins by a decrease in FRET from mTurquoise to cpVenus (*40*). Expression of the three subunits ($G\alpha_q$-127-mTqΔ6, cpVenus-$G\gamma_2$, and untagged $G\beta_1$) of the heterotrimeric G protein from a single plasmid aims to provide equal amounts of the subunits. Single-cell FRET experiments were performed by using HEK293 cells cotransfected with V5-FZD_5 and $G\alpha_q$-127-mTqΔ6 + cpVenus-$G\gamma_2$. As observed in BRET experiments, the addition of WNT-5A led to a decrease in FRET between $G\alpha_q$-mTurquoiseΔ6 and $G\gamma_2$-cpVenus (Fig. 3C and fig. S4A). No change in the FRET ratio was observed when V5-FZD_5 was not cotransfected with $G\alpha_q$-127-mTqΔ6 + cpVenus-$G\gamma_2$, indicating that the dissociation of these G proteins depended on WNT-5A–mediated activation of FZD_5 and did not occur in response to WNT-5A–mediated activation of endogenous FZDs. FRET experiments were also performed in 96-well plates using different concentrations of WNT-5A to generate concentration-dependent response curves. These experiments yielded an EC_{50} value of 509 ng/ml for $G\alpha_q$-127-mTqΔ6 + cpVenus-$G\gamma_2$ in

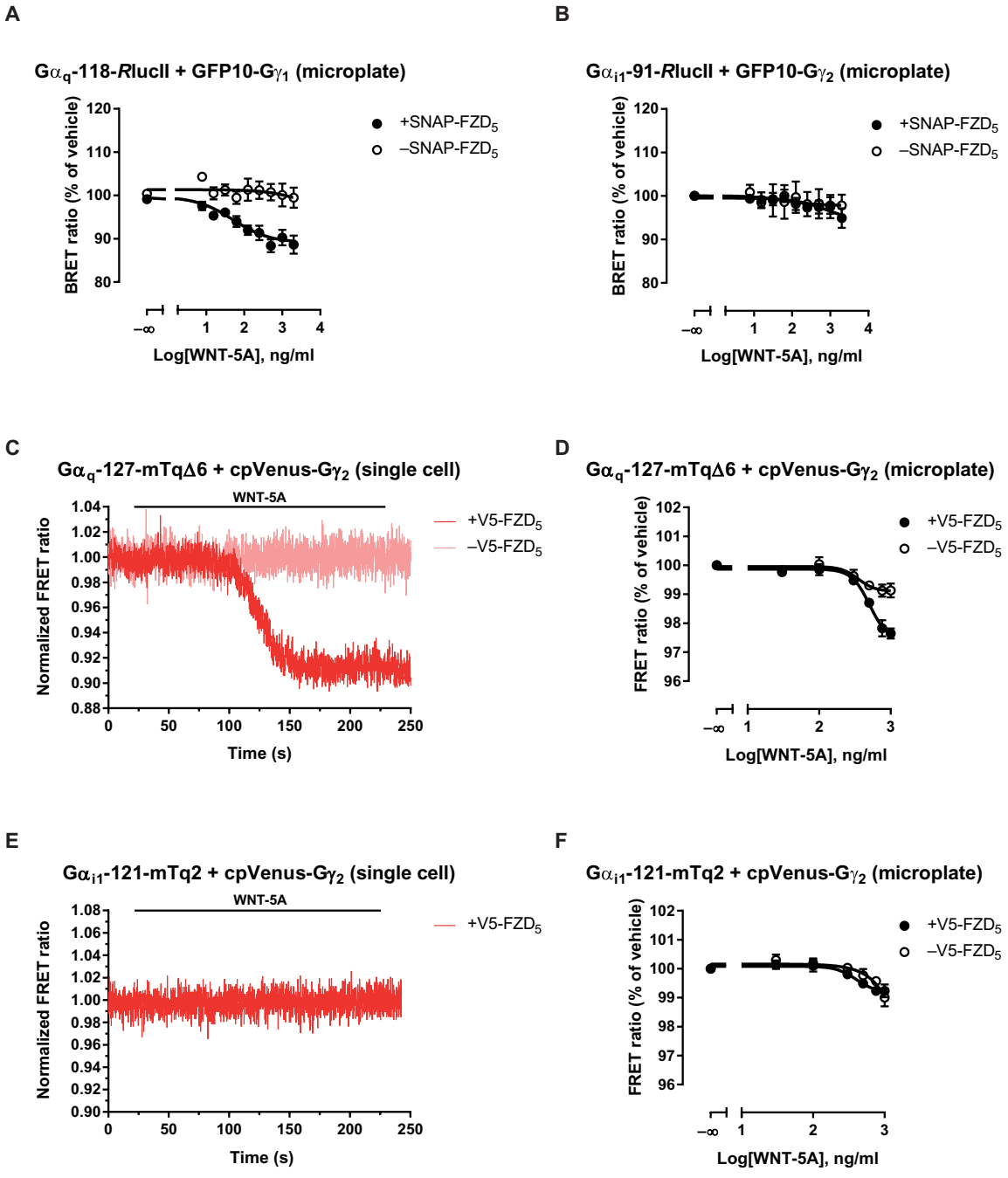

Fig. 3. WNT-5A induces an FZD_5-dependent structural rearrangement of the $G\alpha_q$-$G\beta_1\gamma_1$ interface. (**A** and **B**) BRET experiments in HEK293 cells coexpressing either $G\alpha_q$-118-*R*lucII and GFP10-$G\gamma_1$ (A) or $G\alpha_{i1}$-118-*R*lucII and GFP10-$G\gamma_2$ (B) in the presence or absence of SNAP-FZD_5. Cells were stimulated with the indicated concentrations of recombinant WNT-5A for 5 min before measuring the ratio between GFP10 and *R*lucII. Data are represented as means ± SEM of $n = 3$ to 6 independent experiments conducted at least in duplicate. (**C** and **D**) FRET in HEK293 cells expressing $G\alpha_q$-127-mTqΔ6, $G\beta_1$, and cpVenus-$G\gamma_2$ with or without V5-FZD_5 and stimulated with recombinant WNT-5A approximately 15 to 20 s beginning of the recording. FRET ratios (Venus/Turquoise) from a representative single cell stimulated with recombinant WNT-5A (1000 ng/ml) (C) and from 96-well plates (D) are shown. Data are represented as means ± SEM of $n = 3$ independent experiments conducted in quadruplicate. (**E** and **F**) FRET experiments in HEK293 cells expressing $G\alpha_{i1}$-121-mTq2, $G\beta_1$, and cpVenus-$G\gamma_2$ with and without V5-FZD_5 and stimulated with recombinant WNT-5A approximately 15 to 20 s at the beginning of the recording. FRET ratios (Venus/Turquoise) from a representative single cell stimulated with recombinant WNT-5A (1000 ng/ml) (E) and from 96-well plates stimulated with the indicated concentrations of WNT-5A. Data are represented as means ± SEM of $n = 3$ independent experiments conducted at least in quadruplicate.

the presence of V5-FZD_5 (Fig. 3D). The return of the FRET signal to baseline indicated the transient nature of $G\alpha_q$ activation after WNT stimulation (fig. S4B). In line with the BRET data, no FZD_5-induced activation of $G\alpha_{i1}$ could be detected using the FRET sensor $G\alpha_{i1}$-121-mTq2 + cpVenus-$G\gamma_2$ (*41*), either in single cells (Fig. 3E and fig. S4C) or in 96-well plates (Fig. 3F).

The open, active conformation of classical GPCRs is induced by agonist binding and stabilized by heterotrimeric G proteins. In the case of FZDs, several intracellular effectors interact with the receptor and could potentially contribute to the agonist-induced conformational changes (Fig. 1). FZD_5 has also been described to recruit the phosphoprotein Dishevelled (DVL) (*15*, *42*), and thus, the question arose whether DVL binding could also contribute to the observed ligand-induced conformational changes. Before evaluating the interaction between the FRET probes and DVL, we first determined whether the FZD_5 FRET sensor was capable of activating G proteins similarly to V5-FZD_5 by cotransfecting HEK293 cells with either V5-FZD_5-FlAsH436 or V5-FZD_5-FlAsH439 plus the $G\alpha_q$ FRET sensor ($G\alpha_q$-mTurquoiseΔ6 and $G\gamma_2$-cpVenus). Both V5-FZD_5-FlAsH constructs lacking the C-terminal CFP activated $G\alpha_q$ to a similar extent as the wild-type receptor V5-FZD_5 (fig. S5A), which suggests that the FZD_5 sensor retains its functionality. Next, we investigated the interaction between the FZD_5 FRET probes and DVL. FLAG-DVL1 was coexpressed in HEK293 cells with V5-FZD_5, V5-FZD_5-CFP, or V5-FZD_5-FlAsH436-CFP, and the subcellular localization of DVL was evaluated by confocal microscopy (fig. S5B). Both V5-FZD_5 and V5-FZD_5-CFP recruited DVL to the PM, whereas V5-FZD_5-FlAsH436-CFP was not capable of mediating this recruitment. A similar pattern was observed and quantified when coexpressing DVL2-GFP with the various forms of FZD_5 and the FZD_5 FRET sensors (fig. S5, C to E). Therefore, we concluded that the insertion of the FlAsH-binding motif in IL3, a known interaction site for DVL (*15*), prevented the interaction between FZD_5 and DVL. This provides further evidence for a link between heterotrimeric G proteins, but not DVL, and the observed agonist-induced FRET changes in either V5-FZD_5-FlAsH436-CFP or V5-FZD_5-FlAsH439-CFP. Nevertheless, the functionality of

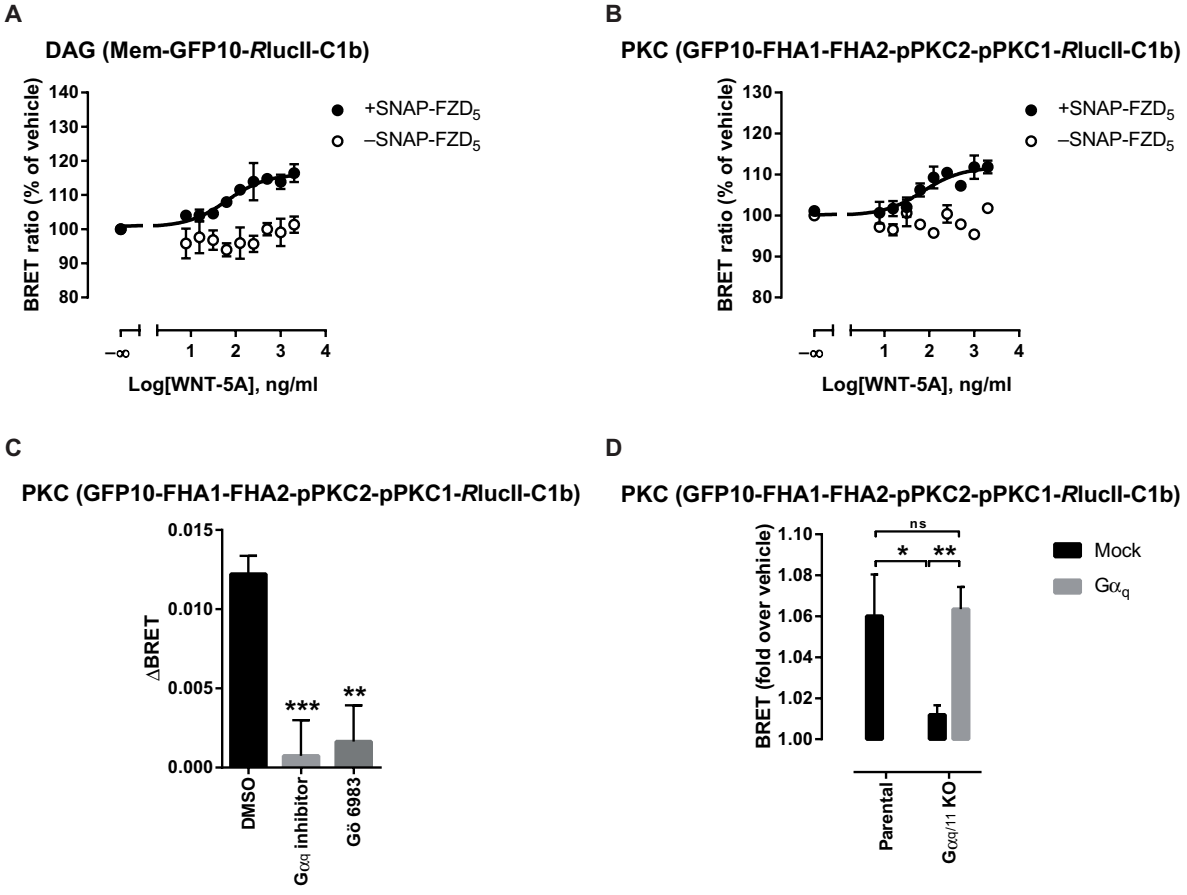

Fig. 4. WNT-5A–mediated stimulation of FZD_5 induces $G\alpha_q$-dependent downstream signaling. (**A**) BRET experiments in HEK293 cells expressing the DAG biosensor (Mem-GFP10-*R*lucII-C1b) alone or with SNAP-FZD_5. Cells were stimulated with the indicated concentrations of recombinant WNT-5A before measuring the ratio between GFP10 and *R*lucII fluorescence. Data are represented as means ± SEM of $n = 3$ to 6 independent experiments conducted at least in duplicate. (**B**) BRET experiments in HEK293 cells expressing the PKC biosensor (GFP10-FHA1-FHA2-pPKC2-pPKC1-*R*lucII-C1b) alone or with SNAP-FZD_5. Cells were stimulated with the indicated concentrations of recombinant WNT-5A before measuring the ratio between GFP10 and *R*lucII fluorescence. Data are represented as means ± SEM of $n = 3$ to 6 independent experiments conducted at least in duplicate. (**C**) HEK293 cells expressing the PKC biosensor and SNAP-FZD_5 were pretreated with the $G\alpha_q$ inhibitor YM-294890 or the PKC inhibitor Gö 6983 before being stimulated with WNT-5A (2000 ng/ml). Data are expressed as the difference in BRET ratio with and without ligand (ΔBRET). Data are represented as means ± SEM of $n = 3$ to 10 independent experiments conducted at least in duplicate. $^{**}P < 0.01$ and $^{***}P < 0.0001$ [one-way analysis of variance (ANOVA) with Fisher's least significant difference (LSD) post hoc analysis]. DMSO, dimethyl sulfoxide. (**D**) BRET experiments in parental and $G\alpha_{q/11}$ KO HEK293 cells expressing the PKC biosensor and SNAP-FZD_5. Cells were stimulated with WNT-5A (2000 ng/ml) in the presence or absence of a transgene encoding $G\alpha_q$. Mock treatment transfection with empty vector DNA instead of $G\alpha_q$. Data are expressed as the fold change in BRET over vehicle. Data are represented as means ± SEM of $n = 5$ independent experiments conducted at least in duplicate. $^{*}P < 0.05$ and $^{**}P < 0.01$ (two-tailed *t* test).

the wild-type FZD_5 with regard to ligand-induced G protein activation and DVL interaction [fig. S5, C to E and (*15*)] argues that FZD_5 can interact with both DVL and heterotrimeric G proteins.

$G\alpha_q$-dependent induction of second messengers and activation of downstream kinases in response to WNT-5A–evoked FZD_5 activation

Activation of the $G\alpha_q$ signaling pathway leads to the production of inositol 1,4,5-trisphosphate (IP_3) and DAG by phospholipase C (PLC), the intracellular release of Ca^{2+} from the endoplasmic reticulum, the activation of PKC, and subsequently the extracellular signal–regulated kinase 1 (ERK1) and ERK2 (ERK1/2) pathway (*43*). To determine whether WNT-5A–FZD_5–$G\alpha_q$ activated this intracellular cascade, we systematically assayed the activation of the aforementioned secondary messengers and kinases using live-cell spectrometric measurements and biochemical approaches. First, we used an artificial BRET-based biosensor that measures the production of DAG (*44*). The biosensor encodes an N-terminal GFP10, a C-terminal *R*lucII, the plasma-targeting CAAX motif from the tyrosine kinase Lyn, a flexible linker, and the DAG-binding domain C1b from PKCδ. Tethered to the membrane by myristoyl and palmitoyl groups at the N terminus of GFP10, the biosensor folds upon itself after PLC activation through binding of C1b to the DAG-enriched membrane, resulting in an increase in intramolecular BRET. The addition of WNT-5A to HEK293 cells coexpressing SNAP-FZD_5 and the DAG BRET sensor led to a dose-dependent increase in BRET, indicative of the production of DAG with a similar EC_{50} value to that of $G\alpha_q$ activation (64 ng/ml) (Fig. 4A). No increase in the DAG sensor BRET signal was observed upon WNT-5A stimulation of cells lacking SNAP-FZD_5, confirming the specificity of the signal.

To probe signaling downstream of DAG production, we made use of another BRET-based biosensor that measures PKC activation. This sensor encodes an N-terminal GFP10, two phosphosensing forkhead-associated domains 1/2 (FHA1 and FHA2), which are separated from two PKC phosphosubstrates by a flexible linker, and followed by *R*lucII and C1b at the C terminus. Upon phosphorylation of the phosphosubstrates by PKC, the biosensor folds upon itself to bring *R*lucII and GFP10 in proximity to one another in like fashion to the DAG biosensor. As expected, WNT-5A stimulation of SNAP-FZD_5–expressing HEK293 cells led to a dose-dependent increase in the activation of the PKC (EC_{50} = 72 ng/ml; Fig. 4B). To determine whether this activation depended on $G\alpha_q$, we tested the effect of the $G\alpha_q$ inhibitor YM-254890. YM-254890 nearly completely inhibited the WNT-5A–induced PKC sensor response (Fig. 4C). Similarly, pretreatment with the PKC inhibitor Gö 6983 decreased the PKC sensor response to WNT-5A, arguing for FZD_5-mediated PKC activation (Fig. 4C). Although this confirmed our hypothesis pharmacologically, this did not confirm that the WNT-5A–induced PKC activation through FZD_5 depended exclusively on $G\alpha_q$. To address this, we used HEK293 cells lacking $G\alpha_{q/11}$ (*45*). Compared to parental HEK293 cells, $G\alpha_{q/11}$ knockout ($G\alpha_{q/11}$ KO) cells expressing SNAP-FZD_5 and the PKC biosensor did not respond to WNT-5A stimulation, suggesting that the PKC activation observed in the wild-type HEK293 cells resulted from FZD_5-mediated activation of the $G\alpha_{q/11}$ subfamily of heterotrimeric G proteins (Fig. 4D). Supporting this conclusion, the lack of response observed in the $G\alpha_{q/11}$ KO cells was rescued by the transgenic expression of $G\alpha_q$ in these cells, resulting in a response comparable to those of wild-type HEK293 cells (Fig. 4D).

Involvement of endogenous $G\alpha_q$ signaling in cellular responses to WNT-5A–FZD_5 signaling

Whereas the aforementioned measures of GPCR activation rely on fluorescent labels for measuring individual pathways, label-free DMR technology offers a pathway-unbiased "holistic" view of GPCR signaling. It allows detection of integrated responses in real time by optical measurement of changes in refractive index that occur when cells are exposed to pharmacologically active stimuli (*46*). Here, we compared the DMR response profiles of WNT-5A–stimulated HEK293 cells stably expressing V5-FZD_5-CFP and the parental cells used to derive the expression line. Cells expressing V5-FZD_5-CFP exhibited a positive DMR response to WNT-5A that was both transient and dose dependent (Fig. 5A). These activity profiles were abolished by preincubation of cells with the $G\alpha_q$ inhibitor FR900359 (Fig. 5B). Stimulating the parental HEK293 cells with WNT-5A did not elicit any DMR changes regardless of the absence (Fig. 5C) or presence (Fig. 5D) of FR900359. All real-time traces are quantified as area under the curve (AUC) from 0 to 2000 s (Fig. 5E). As a means of controlling for the general responsiveness of V5-FZD_5-CFP–expressing and parental HEK293 cells, endogenous muscarinic receptors and epidermal growth factor (EGF) receptors were stimulated with carbachol and EGF, respectively, in the presence or absence of the $G\alpha_q$ inhibitor FR900359 (fig. S6, A to D). Real-time traces from cells treated with carbachol (fig. S6E), forskolin (fig. S6F), and EGF (fig. S6G) were used to quantify the maximum response from 0 to 2000 s, demonstrating that only G_q-coupled muscarinic receptors were sensitive to FR900359.

The role of $G\alpha_q$ signaling in pancreatic cancer cells

Having found that FZD_5 interacted with $G\alpha_q$ and activated the $G\alpha_q$-PLC pathway in an overexpression system, we investigated the functional relevance of this signaling pathway in a more physiologically relevant cell type. To this end, we took advantage of the discovery that a subset of pancreatic ductal adenocarcinoma cells (PDACs) depends on FZD_5 for proliferation (*14*). Human PDAC HPAF-II cells carry a homozygous loss-of-function mutation in *RNF43* and depend on WNT signaling for proliferation and survival. To determine whether these cells were capable of generating a $G\alpha_q$-mediated response to WNT-5A, we measured the intracellular Ca^{2+} in WNT-5A–stimulated HPAF-II cells using a fluorescent calcium indicator and fluorescence imaging plate reader (FLIPR). The addition of WNT-5A led to an increase in fluorescence, indicative of Ca^{2+} mobilization that was inhibited by the $G\alpha_q$ inhibitor YM-254890 (Fig. 6, A and B), suggesting that WNT-5A induced $G\alpha_q$ signaling through endogenous FZDs. The addition of WNT-3A, but not WNT-5A, to HPAF-II cells led to the phosphorylation of low-density lipoprotein receptor-related protein 6 or the stabilization of β-catenin, common measures of WNT–β-catenin signaling (fig. S7A). Both WNT-3A and WNT-5A induced an electrophoretic shift, indicative of phosphorylation of DVL2 in HPAF-II cells (fig. S7B). Therefore, both WNT-3A and WNT-5A elicited DVL phosphorylation, but only WNT-3A stimulated WNT–β-catenin signaling, whereas WNT-5A induced only WNT-Ca^{2+} signaling. Given the requirement for FZD_5 for proliferation of HPAF-II cells, we asked whether signaling through $G\alpha_q$ was also required for the survival of these cells. As had been previously reported (*14*), inhibition of the *O*-acyltransferase PORCN, which is involved in processing of WNT ligands, using the compound C59 {2-[4-(2-methylpyridin-4-yl)phenyl]-*N*-[4-(pyridin-3-yl)phenyl] acetamide} resulted in a marked decrease in cellular viability (Fig. 6C).

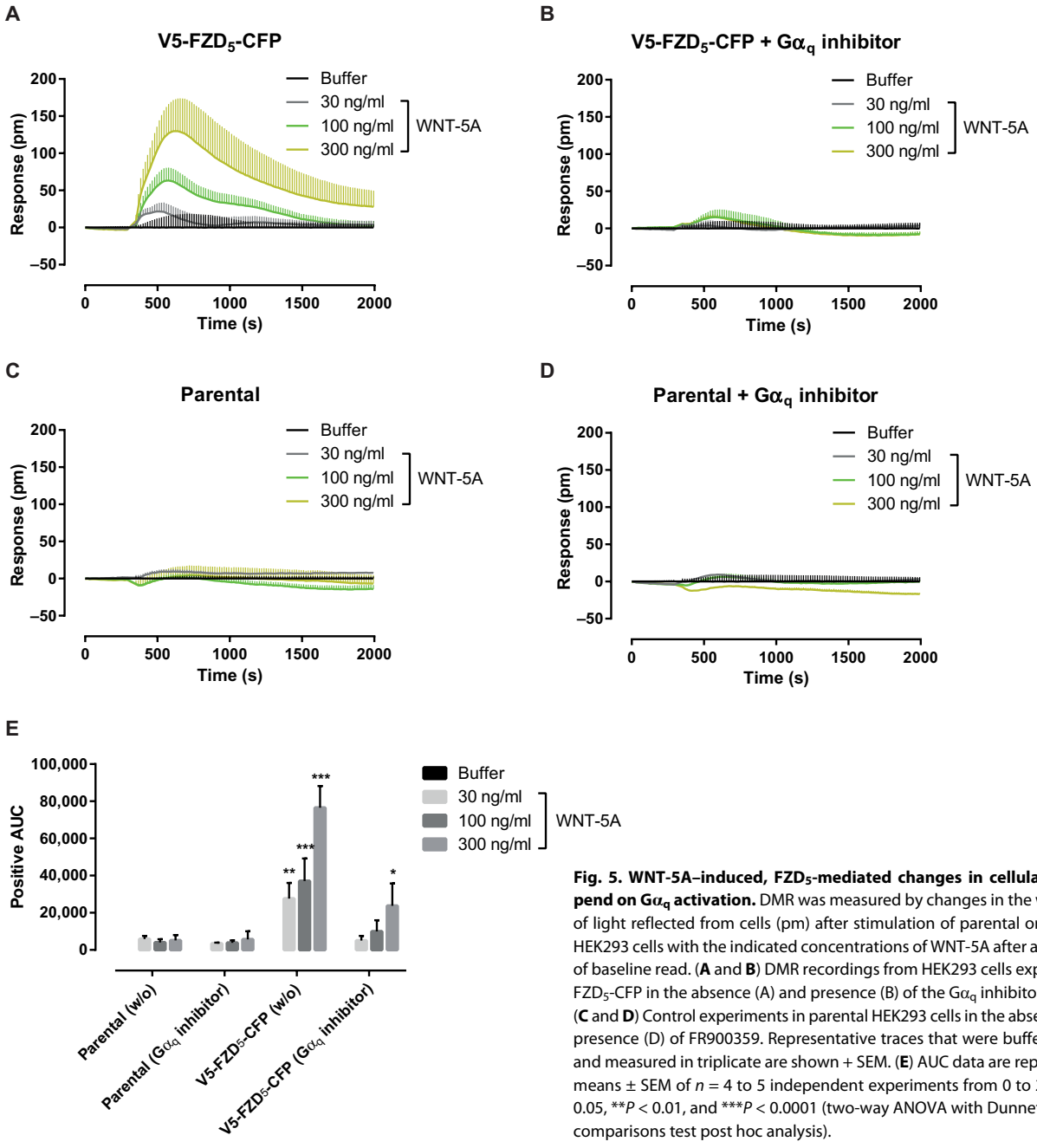

Fig. 5. WNT-5A–induced, FZD_5-mediated changes in cellular DMR depend on $G\alpha_q$ activation. DMR was measured by changes in the wavelength of light reflected from cells (pm) after stimulation of parental or transgenic HEK293 cells with the indicated concentrations of WNT-5A after at least 200 s of baseline read. (**A** and **B**) DMR recordings from HEK293 cells expressing V5-FZD_5-CFP in the absence (A) and presence (B) of the $G\alpha_q$ inhibitor FR900359. (**C** and **D**) Control experiments in parental HEK293 cells in the absence (C) and presence (D) of FR900359. Representative traces that were buffer-corrected and measured in triplicate are shown + SEM. (**E**) AUC data are represented as means ± SEM of $n = 4$ to 5 independent experiments from 0 to 2000 s. $^*P < 0.05$, $^{**}P < 0.01$, and $^{***}P < 0.0001$ (two-way ANOVA with Dunnett's multiple comparisons test post hoc analysis).

Similarly, incubation of HPAF-II cells with the $G\alpha_q$ inhibitor FR900359 also led to a decrease in cellular proliferation compared to vehicle alone (Fig. 6C). Moreover, the PORCN inhibitor–resistant cell line PANC-1, which has been shown to not require FZD_5 for survival (*14*), was insensitive to $G\alpha_q$ inhibition (Fig. 6D).

DISCUSSION

In the current study, we provide evidence that FZD_5 is a prototypical GPCR using live-cell assays that address the GPCR hallmarks of FZD_5 at the levels of receptor activation, signal initiation, and signal propagation. On the basis of known movements of transmembrane domains of GPCRs and homology models of FZD_5 in active and inactive conformations, we developed a FRET-based sensor capable of monitoring ligand-induced conformational changes in FZD_5. The changes in FRET in FZD_5 resemble those of other prototypical GPCRs where the same approach has been used (*25*, *27*, *30*). In accordance with previously published FRET probes for other GPCRs, FZD FRET probes turned out to be valuable tools for assessing ligand-induced conformational changes and activation kinetics, suggesting that class F GPCRs share homologous activation mechanisms with prototypical GPCRs. The FZD FRET probes exhibited slower activation kinetics in response to binding to WNT compared to class A receptors in response to small-molecule ligands. We do not yet have the tools and

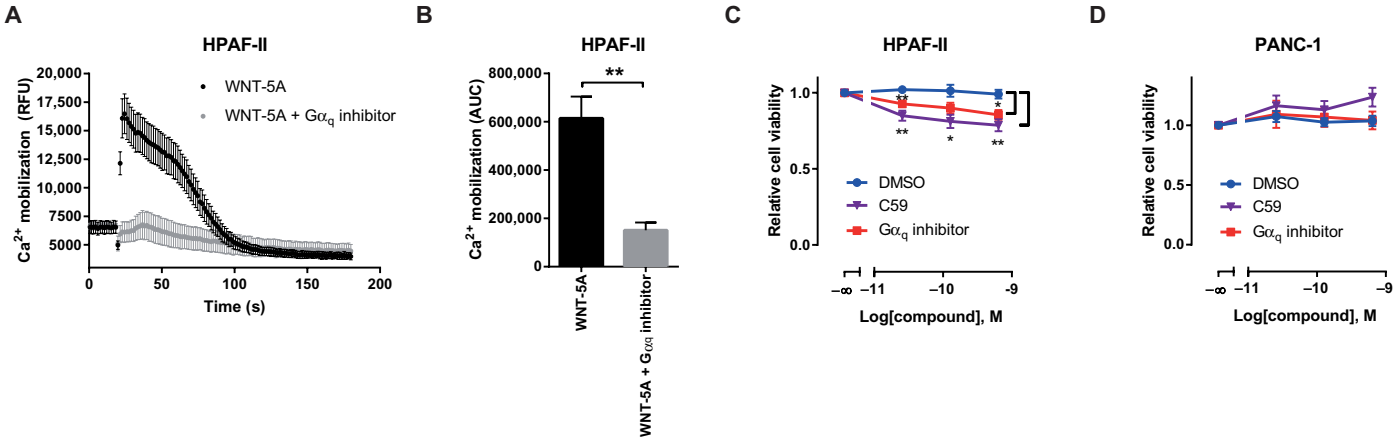

Fig. 6. WNT-5A–FZD–Gα$_q$ signaling in PDACs. (**A**) Intracellular Ca^{2+} in HPAF-II cells was measured after the application of recombinant WNT-5A in the presence and absence of the Gα$_q$ inhibitor YM-254890. RFU, relative fluorescence units. (**B**) Quantification and statistical analysis of AUC from experiments in (A). Data are represented as means ± SEM of $n = 3$ independent experiments conducted in duplicate. $^{**}P < 0.01$ (two-tailed t test). (**C** and **D**) Cell viability assays in HPAF-II and PANC-1 cells using the indicated concentrations of the PORCN inhibitor C59 and the Gα$_q$ inhibitor FR900359. Data are represented as means ± SEM of $n = 3$ to 4 independent experiments conducted in triplicate. $^{*}P < 0.05$ (two-tailed t test).

technology to dissect these kinetic differences and can only speculate that the interaction of WNTs with components of the extracellular matrix (ECM) may affect receptor binding and ultimately activation kinetics (*1*). Our dcFRAP experiments revealed that FZD_5 interacts with Gα$_q$. This type of approach has previously been used to probe for the interaction of heterotrimeric G proteins with FZD_4, FZD_6, and FZD_{10} (*35*, *47*, *48*), as well as cannabinoid CB_1 (*35*) and muscarinic acetylcholine M_3 receptors (*49*). Ligand-induced activation of the Gα$_q$-PLC pathway as measured by RET and fluorescent indicator-based techniques revealed that FZD_5 functionally activated Gα$_q$, led to the production of DAG, induced the release of Ca^{2+} from intracellular stores, and increased the activation of endogenous PKC. It is important to note that the experiments monitoring DAG, Ca^{2+}, and PKC all relied on endogenous Gα$_{q/11}$. These findings were confirmed and integrated in global, WNT-induced whole-cell activity profiles using DMR and clearly indicated that WNT-5A evoked an FZD_5-selective and G_q inhibitor–sensitive cellular response.

Because of the chemical nature of WNT proteins and the difficulties in obtaining purified, active protein with defined specific activity, quantitative pharmacological information is sparse (*50*, *51*). Here, we aimed to reproducibly generate dose-response relationships in various assays. When comparing the potency of agonist-induced receptor conformational changes with the G_q BRET probes, the leftward shift in the dose-response curve for the latter can be explained by amplification downstream of receptor activation [fig. S8 and (*25*)] (*52*). Consistent with a signal amplification mechanism, as known for classical G protein coupling, ligand concentrations leading to partial receptor activation (fig. S3B) resulted in full Gα$_q$ activation (fig. S4B). On the other hand, the differences in potency between the FRET and BRET G protein probes could, for example, originate from the different βγ subunit combinations used in the two experimental paradigms (*53*). However, other more subtle factors cannot be excluded, such as differences in the abundance of the receptor or G protein in the different experimental paradigms, which would result in a different acceptor/donor ratio, leading to a shift in the EC_{50} value (*54*). Quantifying pharmacological parameters in the WNT-FZD system can also be influenced by a multistep binding mode as summarized by recent publications on class B GPCRs (*55*) or receptor occupancy in cytomegalovirus promoter–mediated expression systems compared to systems relying on endogenous receptors. A multistep binding mode would also account for the delayed onset of receptor activation as seen for the FZD_5 FRET sensors (Fig. 1F).

The repertoire of readouts that we described in this study could be used to discover FZD-targeting drugs. Both BRET and FRET technologies are amenable to high-throughput screening (*56*), and their use in studying receptor-induced G protein activation represents a previously underappreciated angle that might open the door to understanding FZD pharmacology.

Although technological developments assist in understanding WNT-FZD signaling to heterotrimeric G proteins mechanistically, growing evidence also highlights the physiological importance of G protein–dependent WNT signaling. For example, it has been shown that heterotrimeric G proteins are required to transduce mammalian WNT signaling in primary microglia, synaptic development, and inhibition of osteoclast differentiation (*57*–*60*). Difficulties in studying G protein signaling downstream of FZDs arise in part from the fact that WNTs and FZDs are ubiquitously present in tissues and cells, and determining the origin and minimal functional unit of a particular signaling cascade without small-molecule inhibitors has not been without its hurdles. With the advent of CRISPR-Cas9 gene editing, it is now possible to carry out genome-wide screens that do not only unravel signaling networks but also reveal vulnerabilities in tumors. Using this approach, FZD_5 was found to be required for the proliferation of PDAC cells (*14*). Our findings indicated that inhibition of Gα$_q$ blocks WNT-mediated Ca^{2+} mobilization, a second messenger system intrinsically linked to proliferation, in PDAC cells. Furthermore, G_q inhibition reduced the viability of these cells in culture. Thus, given the proliferative requirement for FZD_5 in these cells and the fact that this effect is WNT mediated, FZD_5-G_q signaling is potentially another avenue that could be exploited to treat patients afflicted by this disease.

The present study provides a comprehensive characterization of the GPCR nature of a FZD by demonstrating agonist-induced conformational changes, interaction with heterotrimeric G_q proteins, ligand-induced and FZD-mediated activation of G proteins, and G

protein–dependent downstream signaling. In summary, the understanding of the role of FZD_5, not only as a receptor mediating WNT–β-catenin signaling but also as a GPCR, offers exciting opportunities for targeting this and other FZDs therapeutically.

MATERIALS AND METHODS

Molecular modeling

A homology model of inactive mouse FZD_5 (UniProt ID: Q9EQD0) was generated using a crystal structure of SMO as template (PDB ID: 5V56) (*28*). To obtain a model of FZD_5 in an active conformation, TM6 (residues 445 to 467) was modeled on the basis of the crystal structure of the β_2AR in complex with G_s (PDB ID: 3SN6) (*20*). Because of the lack of suitable template, the N- and C-terminal regions (amino acids 1 to 228 and 541 to 585) were excluded from the models. Initial sequence alignments were generated using ClustalX2 (*61*), and homology models were constructed using Modeller 9.16 (*62*). A set of 100 homology models was generated for both the active and inactive conformations of FZD_5. A representative model was selected among the 10 structures with the best discrete optimized protein energy (DOPE) scores (*63*) based on visual inspection.

Cell culture and transfections

HEK293, HPAF-II, and PANC-1 cells (American Type Culture Collection) were cultured in Dulbecco's modified Eagle's medium (DMEM) supplemented with 10% fetal bovine serum, 1% penicillin/streptomycin, and 1% L-glutamine (all from Invitrogen Technologies) in a humidified CO_2 incubator at 37°C. $G\alpha_{q/11}$ KO HEK293 cells were a gift from A. Inoue (Tohoku University, Japan) (*45*). All cell culture plastics were from Sarstedt, unless otherwise specified. For dcFRAP experiments, cells were seeded on 35-mm ECM gel–coated (1:300; Sigma-Aldrich) glass-bottom dishes (Greiner Bio-One four-compartment 35-mm glass-bottom dishes). Cells were transfected with Lipofectamine 2000 24 hours before analysis. For FRET efficiency measurements and FZD-mediated DVL recruitment, cells were seeded onto round 24-mm coverslips precoated with poly-D-lysine in six-well plates. Cells were transfected 4 to 5 hours later using the Effectene transfection reagent (Qiagen). Cell culture medium was replaced 16 to 18 hours later, and the analysis was done 48 hours after transfection. To investigate the cellular expression of the receptor sensors or their FRET efficiency, 500 ng of DNA per well of each sensor was used for transfection. HEK293 cells stably expressing the sensor V5-FZD_5-FlAsH436-CFP were also used for the experiments following the same procedure. For FRET efficiency control experiments, cells were cotransfected with 300 ng of V5-FZD_5-CFP and 300 ng of V5-FZD_5-FlAsH. Pharmacological inhibition of $G\alpha_q$ signaling was accomplished with structurally related compounds 1 μM FR900359 (*64*) or 100 nM YM-254890 (Wako Laboratory Chemicals). PKC inhibition was achieved with 100 nM Gö 6983 (Sigma-Aldrich). C59 was used to inhibit PORCN to reduce endogenous secretion of WNTs (*65*). For stimulation, recombinant WNT-5A (645-WN; R&D Systems/Bio-Techne) was used.

Immunocytochemistry

Round glass coverslips (13 mm) were placed in 24-well plates and coated for 30 min with 0.1% gelatin. After that time, gelatin was removed and the wells were left to dry for 1 hour at room temperature. HEK293 stably expressing the receptor constructs were seeded onto these coverslips at a density of 100,000 cells per well. Twenty-four hours later, cells were transfected with 100 ng per well of DVL1-FLAG using Lipofectamine 2000. The next day, cells were fixed with 4% paraformaldehyde in phosphate-buffered saline (PBS) and incubated overnight with mouse anti-FLAG M2 (1:500; Sigma-Aldrich). Secondary antibody incubation was carried out for 40 min with Cy3 anti-mouse (1:500; Jackson ImmunoResearch Laboratories Inc.). After washing, cells were incubated for 5 min with 4′,6-diamidino-2-phenylindole (DAPI) at room temperature in the dark. Last, coverslips were mounted with glycerol gelatin (Sigma-Aldrich).

FZD_5 constructs

To generate the construct V5-FZD_5-CFP, V5-FZD_5 was amplified by polymerase chain reaction (PCR) (forward primer: 5′-atctggtgggtcatcctgtc-3′; reverse primer: 5′-ctgatgtctagatacgtgcgacagggacacttg-3′) and subcloned into CFP-pcDNA3 between the Hind III and Xba I restriction sites. To create the FRET-based receptor sensors, the six amino acids of the FlAsH-binding sequence CCPGCC (5′-tgttgcccgggctgctgt-3′) were inserted within the third intracellular loop of FZD_5 by standard overlapping PCR reactions. For the sensor V5-FZD_5-FlAsH436-CFP, the motif was introduced between the amino acids Gly^{436} and Gly^{437} using the following forward primers (1 to 3) 5′-tgttgcccgggctgctgtggcactaagacggacaagcta-3′, 5′-agcgtcatcaagcaggttgttgcccgggctgctgtg-3′, and 5′-tcactcttccgcatccggagcgtcatcaagcaggttgt-3′ and the following reverse primer: 5′-ctgatgtctagatacgtgcgacagggacacttg-3′. For the sensor V5-FZD_5-FlAsH439-CFP, the FlAsH-binding motif was introduced between the amino acids Lys^{439} and Thr^{440} using the following forward primers (1 to 3): 5′-tgttgcccgggctgctgtacggacaagctagagaagctc-3′, 5′-aagcagggtggcactaagtgttgcccggggctgctgtacg-3′, and 5′-cgcatccggagcgtcatcaagcagggtggcactaagtgt-3′ and the following reverse primer: 5′-ctcactctagatacgtgcgacag-3′. To generate the constructs without CFP (V5-FZD_5-FlAsH436 and V5-FZD_5-FlAsH439), the region containing the FlAsH-binding motif was inserted into the V5-FZD_5 plasmid between the Hind III and BstX I restriction sites. To create V5-FZD_5-mCherry, a Bgl II site was cloned behind the Hind III site and an Age I site was placed in front of the Xba I restriction site in V5-FZD_5-CFP. To add the Bgl II site, a forward primer (5′-cagtaagcttagatctaccatggtcccgtgcacgctg-3′) and a reverse primer (5′-gtgcgcaccttgttgtagag-3′) were used. To add the Age I site, the following forward and reverse primers were used: 5′-cagtgtcaagtccattacgg-3′ and 5′-agcagtaccggttgtacgtgcgacagggacacttg-3′, respectively. From this, V5-FZD_5 was subcloned into pmCherry-N1 between the Bgl II and Age I restriction sites. To create SNAP-FZD_5-*R*luc8, SNAP-FZD_5 was cloned into p*R*luc8-N1 using the following primers and inserted with Hind III and Age I restriction sites: forward, 5′-gacaagcttgccaccatggtcccgtgcacgctgctcctg-3′; reverse, 5′-cgtaccggtgctacgtgcgacagggacacttgcttgtggtatgc-3′.

Description of the sensors

To evaluate the activation of G proteins, previously described FRET and BRET sensors for $G\alpha_q$ and $G\alpha_{i1}$ were used (*40*, *41*). For FRET, each sensor consists of a single plasmid encoding the three subunits of the heterotrimeric G protein expressed separately: Gα fused to mTurquoise, untagged $G\beta_1$, and $G\gamma_2$ fused to cpVenus. For BRET-based sensors, the $G\alpha_q$-118-*R*lucII and $G\gamma_1$-GFP10 (*36*) and the $G\alpha_{i1}$-91-*R*lucII and $G\gamma_2$-GFP10 (*33*) were used to monitor the activation of G_q and G_{i1}, respectively. In both cases, the biosensor components were coexpressed with $G\beta_1$. The DAG biosensor consists of *R*lucII at the N terminus, followed by the PM-targeting sequence CAAX from Lyn, a flexible linker, the C1b DAG-binding domain from PKCδ, and, last, GFP10 at the C terminus. The PKC sensor is composed of

*R*lucII at the N terminus, followed by two phosphosensing domains (FHA1 and FHA2), a flexible linker, two PKC phosphosubstrates, and GFP10 at the C terminus. Details of the construction and validation of the latter two biosensors can be found in Namkung *et al.* (*44*).

Generation of stable cell lines

To create stable HEK293 cells expressing the receptor sensor V5-FZD_5-FlAsH436-CFP or V5-FZD_5-FlAsH439-CFP, cells were transfected using the Effectene reagent (Qiagen) according to the manufacturer's instructions. Forty-eight hours after seeding and for a period of 2 weeks, culture medium was replaced every day with medium supplemented with geneticin (G-418) (500 μg/ml) to select for transfected cells. Individual colonies were selected and characterized using confocal microscopy. Positive homogeneous cells expressing the desired constructs were maintained in DMEM-containing G-418 (200 μg/ml).

FlAsH labeling

FlAsH labeling was done as previously described (*25*, *29*). Briefly, cells were washed once with Hank's balanced salt solution (HBSS) containing glucose (1.8 g/liter) and then incubated at 37°C for 1 hour with HBSS supplemented with 500 nM FlAsH and 12.5 μM 1,2-ethanedithiol (EDT). After that, cells were rinsed twice with HBSS, incubated for 10 min with HBSS containing 250 μM EDT, and washed again twice with HBSS. Last, cells were maintained in DMEM before measurements.

Förster resonance energy transfer

Fluorescence imaging of FZD_5 FRET sensors was performed as previously described (*25*). Briefly, 5 mM of BAL was used to determine the FRET efficiency of the constructs. This compound removes FlAsH from its binding motif in the receptor, resulting in a dequenching of CFP fluorescence. Coverslips with the cells were mounted using an Attofluor holder (Molecular Probes), and the cells were maintained in imaging buffer. BAL was added to the cells after 20 to 30 s. Recovery of CFP fluorescence was monitored over time, and FRET efficiency was calculated by inputting the minimum and maximum values of CFP into the following equation: $\Delta E/E_{max} \times 100$. Fluorescence intensities data were acquired using Clampex software (Axon Instruments). The FRET ratio is calculated as the fluorescence intensity of FlAsH over that of CFP and subsequently corrected for the signal obtained in vehicle-treated cells.

Single-cell experiments

To investigate the activation of the receptor in single cells, HEK293 cells stably expressing the receptor sensor V5-FZD_5-FlAsH436-CFP were seeded onto WillCo-dish 40-mm glass-bottom dishes precoated with poly-D-lysine. For G protein activation studies, HEK293 cells were seeded onto these plates and transfected 3 to 4 hours later using the Effectene reagent (Qiagen). For transfection, 600-ng DNA of FZD_5 and 200-ng DNA of the G protein FRET sensor were used. Culture medium was replaced 16 to 18 hours later, and cells were incubated overnight with the PORCN inhibitor LGK-974 (Cayman Chemical) at a final concentration of 0.1 μM. Analysis was carried out 48 hours after seeding the cells. To monitor receptor activation, FlAsH labeling of the receptor sensors was performed. Cells were maintained in imaging buffer. The BioPen microfluidic system (Fluicell) was used to deliver the ligands. Recombinant WNT-5A (R&D Systems) was dissolved in imaging buffer containing 0.1% bovine serum albumin (BSA). Saturating concentrations of WNT-5A were used for single-cell experiments: 2000 ng/ml for receptor activation and 1000 ng/ml for G protein activation. Fluorescence intensities data were acquired using Clampex software (Axon Instruments).

Plate reader FRET experiments

To investigate the activation of G proteins in populations of cells, HEK293 cells were seeded in 100-mm plates, and 48 hours later, with a 60 to 70% confluence, cell culture medium was exchanged, and cells were transfected using the Effectene reagent (Qiagen) according to the manufacturer's instructions. For transfection, the following DNA was used per plate: 1.8 μg of V5-FZD_5 or pcDNA3 and 600 ng of the G protein FRET sensor. Twenty-four hours after transfection, black 96-well BRANDplates, flat bottom, were coated for 30 min using poly-D-lysine. After washing with sterile PBS, 30,000 cells were seeded per well. To investigate the activation of the receptor, stable cells expressing the receptor sensor V5-FZD_5-FlAsH436-CFP were seeded in 100-mm plates, and 30,000 cells per well were placed in 96-well plates 72 hours later. Analysis of the cells was done 24 hours after seeding the cells in the 96-well plates using Synergy Neo2 Multi-Mode Microplate Reader (BioTek), with Gen5 Data Analysis Software. Cells were excited at 420 nm, and emission was detected at 485/540 nm. During measurements, cells were maintained at 37°C in imaging buffer containing 0.1% BSA. Recombinant WNT-5A was added to the cells 5 min after the reading started. Fluorescence changes were recorded for an additional 20 min. Data were analyzed using the software GraphPad Prism 6.

Calcium mobilization

Intracellular Ca^{2+} mobilization was measured using the FLIPR Calcium 5 Assay Kit (Molecular Devices). Briefly, HPAF-II cells (350,000 cells/ml) were seeded (48 hours before the assay) onto poly-D-lysine–coated black 96-well culture plates with glass bottom. Cells were loaded with FLIPR calcium 5 indicator dye (Molecular Devices) and incubated with DMSO or $G\alpha_q$ inhibitor (YM-254890; 100 nM) for 60 min and then stimulated with recombinant WNT-5A (2000 ng/ml). Intracellular Ca^{2+} mobilization was detected with the FlexStation II Benchtop Multi-mode Microplate Reader (Molecular Devices).

Confocal microscopy

Confocal analysis of cells was performed using a Leica SP8 microscope and 63× water objective. Coverslips with the cells were mounted using an Attofluor holder (Molecular Probes). To analyze the expression of the receptor constructs and DVL2 recruitment to the membrane, cells were maintained in imaging buffer. CFP was excited using a diode laser at 442-nm laser line, and fluorescence intensities were detected from 450 to 500 nm. GFP was excited using an argon laser at 488-nm laser line and detected at 509 to 600 nm. Images were acquired using 512 × 512 resolution, 400 Hz, a line average of 3, and a frame accumulation of 2. Confocal analysis of the fixed samples was done using a 63× oil-immersion objective. DAPI was excited using a diode 405 laser at 405-nm laser line, and fluorescence intensities were detected at 431 to 480 nm. Cy3 was excited using a diode-pumped solid-state laser at 561-nm laser line and detected at 590 to 679 nm. Images were acquired using 1024 × 1024 resolution, 400 Hz, and a line average of 8.

FRAP, surface cross-linking, and cellular imaging

For dcFRAP experiments, transfected HEK293 cells grown in four-compartment 35-mm glass-bottom dishes were washed three times with BiotinElation buffer (150 mM NaCl, 2.5 mM KCl, 10 mM Hepes, 12 mM glucose, 0.5 mM $CaCl_2$, and 0.5 mM $MgCl_2$) (*66*). Cell-impermeable chemical cross-linking using EZ-Link Sulfo-NHS-Biotin (Thermo

Fisher Scientific) was used to immobilize cell surface proteins. If intracellular proteins are interacting with immobilized cell surface proteins, their respective mobility will be reduced. This setup was used to visualize the assembly of immobilized FZD_5 with heterotrimeric G proteins according to previously published protocols (*35*). Live-cell imaging experiments were carried out using a Zeiss 710 laser scanning microscope. Images were acquired using a 40×, 1.2 numerical aperture C-Apochromat objective, and the 488-nm and the 561-nm laser lines were used to excite GFP/Venus and mCherry fluorophores, respectively. Photobleaching was performed by 100% laser illumination of a 1.80-μm by 1.80-μm area placed over the cell PM. Fluorescence was measured before and after bleaching using low-intensity illumination for a total time period of 100 s. Average pixel intensity was measured using the ZEN2013 software, corrected for background fluctuations and bleaching artifacts, and normalized to prebleached intensity (*67*). The recovered mobile fraction (F_m) was calculated as follows: $F_m = (I_P - I_0) / (I_I - I_0)$, where I_I is the initial intensity measured before bleaching, I_0 is the immediate fluorescence intensity after bleaching, and I_P is intensity value after bleaching. The mobile fraction was defined by the average of the fluorescence recovery assessed between time 85 to 101 s. We excluded experiments in which V5-FZD_5-mCherry was not sufficiently immobilized after the cross-linking procedure (cutoff at 40% cross-linking–induced reduction in mobile fraction).

BRET assay

HEK293 cells were transiently transfected in suspension using Lipofectamine 2000 and seeded onto poly-D-lysine–coated white 96-well cell culture plates with solid bottom (Greiner Bio-One). Forty-eight hours after transfection, cells were washed once with Tyrode's buffer [140 mM NaCl, 2.7 mM KCl, 1 mM $CaCl_2$, 12 mM $NaHCO_3$, 5.6 mM D-glucose, 0.5 mM $MgCl_2$, 0.37 mM NaH_2PO_4, and 25 mM Hepes (pH 7.4)] and maintained in the same buffer. Following the addition of the luciferase substrate coelenterazine 400a, cells were either stimulated with agonist for 5 min for the G protein activity biosensor before reading BRET or stimulated and measured immediately for the DAG and PKC biosensors. BRET was measured using a Synergy Neo microplate reader (BioTek) equipped with acceptor (515 ± 30 nm) and donor (410 ± 80 nm) filters. The BRET signal was determined as the ratio of light emitted by GFP10-tagged biosensors (energy acceptors) and light emitted by *R*lucII-tagged biosensors (energy donors).

DMR assays

DMR assays were performed as described previously (*46*, *68*). Briefly, cells were seeded into 384-well Epic biosensor plates (Corning) at a density of 18,000 cells per well to attain confluency after 24 hours. The following day, cells were washed three times and the medium was changed to starvation medium, lacking fetal calf serum. After 4 hours of incubation in starvation medium (37°C and 5% CO_2), the cells were washed twice with HBSS (Life Technologies) containing 20 mM Hepes (Life Technologies) and were kept for an additional 2 hours in the presence of the $G\alpha_q$ inhibitor FR900359 (*64*) at a final concentration of 1 μM where indicated. Subsequently, at least 3 min of baseline read with the cells subjected to assay buffer (HBSS + 20 mM Hepes adjusted to DMSO) were recorded (no changes in basal DMR) to define a zero-DMR response (DMR in the absence of pharmacological stimuli). Compounds were added using a semiautomatic liquid handling system (SELMA, CyBio). Changes in DMR were monitored for at least 2 hours at 37°C. Raw data were processed using the microplate analyzer plug-in (Corning) for Microsoft Excel and evaluated using the GraphPad Prism software 6.0.

Cell viability assay

HPAF-II and PANC-1 cells were seeded at 1000 to 2000 cells per well in 96-well plates. The next day, cells were treated with the PORCN inhibitor C59, the $G\alpha_q$ inhibitor FR900359, or vehicle in technical triplicate at the indicated concentrations. Medium containing inhibitor or vehicle was replaced every 3 days. Cell viability was measured using Alamar Blue (Thermo Fisher Scientific, catalog no. DAL1025) approximately 6 to 7 days after seeding following the manufacturer's instructions. Fluorescence was measured at 560-nm excitation and 590-nm emission with a SPECTRAmax GEMINI Microplate Spectrofluorometer plate reader (Molecular Devices).

Statistical analysis

Statistical and graphical analyses were performed using GraphPad Prism software unless otherwise indicated. Data were analyzed by two-tailed *t* test or one-way ANOVA with Fisher's LSD post hoc analysis. Curve fitting of FRAP data was done with a two-phase association nonlinear function using the least-squares fit. For single-cell analysis (dcFRAP), the number of the individual ROIs obtained from several cells in at least three independent experiments is provided in the figure legends. Data from individual ROIs are summarized for data presentation, providing the sum of independent observations. Significance levels are given as: $*P < 0.05$, $**P < 0.01$, $***P < 0.001$. All data points throughout the manuscript represent the means ± SEM.

SUPPLEMENTARY MATERIALS

www.sciencesignaling.org/cgi/content/full/11/559/eaar5536/DC1

Fig. S1. Alignment of mouse FZD_5 with the SMO and β_2AR sequences corresponding to the crystal structures used for modeling.

Fig. S2. Validation of V5-FZD_5-FlAsH439-CFP.

Fig. S3. Individual traces from single-cell data and kinetic experiments using V5-FZD_5-FlAsH436-CFP.

Fig. S4. Validation of $G\alpha_q$ and $G\alpha_{i1}$ FRET probes with FZD_5.

Fig. S5. The FZD_5 FRET sensors activate $G\alpha_q$ but do not recruit DVL.

Fig. S6. Control experiments for DMR in HEK293 cells.

Fig. S7. WNT-5A does not activate the WNT–β-catenin pathway in HPAF-II cells.

Fig. S8. Pharmacological properties of receptor activation and stimulation of downstream signaling.

REFERENCES AND NOTES

1. G. Schulte, International union of basic and clinical pharmacology. LXXX. The class Frizzled receptors. *Pharmacol. Rev.* **62**, 632–667 (2010).
2. G. Schulte, V. Bryja, The Frizzled family of unconventional G-protein-coupled receptors. *Trends Pharmacol. Sci.* **28**, 518–525 (2007).
3. A. Koval, V. Purvanov, D. Egger-Adam, V. L. Katanaev, Yellow submarine of the Wnt/Frizzled signaling: Submerging from the G protein harbor to the targets. *Biochem. Pharmacol.* **82**, 1311–1319 (2011).
4. J. P. Dijksterhuis, J. Petersen, G. Schulte, WNT/Frizzled signaling: Receptor-ligand selectivity with focus on FZD-G protein signaling and its physiological relevance: IUPHAR Review 3. *Br. J. Pharmacol.* **171**, 1195–1209 (2013).
5. S. Angers, R. T. Moon, Proximal events in Wnt signal transduction. *Nat. Rev. Mol. Cell Biol.* **10**, 468–477 (2009).
6. T. Ishikawa, Y. Tamai, A. M. Zorn, H. Yoshida, M. F. Seldin, S. Nishikawa, M. M. Taketo, Mouse Wnt receptor gene Fzd5 is essential for yolk sac and placental angiogenesis. *Development* **128**, 25–33 (2001).
7. A. Blumenthal, S. Ehlers, J. Lauber, J. Buer, C. Lange, T. Goldmann, H. Heine, E. Brandt, N. Reiling, The Wingless homolog WNT5A and its receptor Frizzled-5 regulate inflammatory responses of human mononuclear cells induced by microbial stimulation. *Blood* **108**, 965–973 (2006).
8. M. Sen, M. Chamorro, J. Reifert, M. Corr, D. A. Carson, Blockade of Wnt-5A/Frizzled 5 signaling inhibits rheumatoid synoviocyte activation. *Arthritis Rheum.* **44**, 772–781 (2001).

9. X. He, J.-P. Saint-Jeannet, Y. Wang, J. Nathans, I. Dawid, H. Varmus, A member of the Frizzled protein family mediating axis induction by Wnt-5A. *Science* **275**, 1652–1654 (1997).
10. F. Cavodeassi, F. Carreira-Barbosa, R. M. Young, M. L. Concha, M. L. Allende, C. Houart, M. Tada, S. W. Wilson, Early stages of zebrafish eye formation require the coordinated activity of Wnt11, Fz5, and the Wnt/β-catenin pathway. *Neuron* **47**, 43–56 (2005).
11. M. Sahores, A. Gibb, P. C. Salinas, Frizzled-5, a receptor for the synaptic organizer Wnt7a, regulates activity-mediated synaptogenesis. *Development* **137**, 2215–2225 (2010).
12. A. T. Weeraratna, Y. Jiang, G. Hostetter, K. Rosenblatt, P. Duray, M. Bittner, J. M. Trent, Wnt5a signaling directly affects cell motility and invasion of metastatic melanoma. *Cancer Cell* **1**, 279–288 (2002).
13. C. Liu, Y. Wang, P. M. Smallwood, J. Nathans, An essential role for Frizzled5 in neuronal survival in the parafascicular nucleus of the thalamus. *J. Neurosci.* **28**, 5641–5653 (2008).
14. Z. Steinhart, Z. Pavlovic, M. Chandrashekhar, T. Hart, X. Wang, X. Zhang, M. Robitaille, K. R. Brown, S. Jaksani, R. Overmeer, S. F. Boj, J. Adams, J. Pan, H. Clevers, S. Sidhu, J. Moffat, S. Angers, Genome-wide CRISPR screens reveal a Wnt–FZD5 signaling circuit as a druggable vulnerability of *RNF43*-mutant pancreatic tumors. *Nat. Med.* **23**, 60–68 (2017).
15. D. V. F. Tauriello, I. Jordens, K. Kirchner, J. W. Slootstra, T. Kruitwagen, B. A. M. Bouwman, M. Noutsou, S. G. D. Rüdiger, K. Schwamborn, A. Schambony, M. M. Maurice, Wnt/β-catenin signaling requires interaction of the Dishevelled DEP domain and C terminus with a discontinuous motif in Frizzled. *Proc. Natl. Acad. Sci. U.S.A.* **109**, E812–E820 (2012).
16. C. Liu, J. Nathans, An essential role for frizzled 5 in mammalian ocular development. *Development* **135**, 3567–3576 (2008).
17. D. J. Olson, J. L. Christian, R. T. Moon, Effect of wnt-1 and related proteins on gap junctional communication in Xenopus embryos. *Science* **252**, 1173–1176 (1991).
18. M. Audet, M. Bouvier, Restructuring G-protein- coupled receptor activation. *Cell* **151**, 14–23 (2012).
19. G. Lebon, T. Warne, P. C. Edwards, K. Bennett, C. J. Langmead, A. G. W. Leslie, C. G. Tate, Agonist-bound adenosine A_{2A} receptor structures reveal common features of GPCR activation. *Nature* **474**, 521–525 (2011).
20. S. G. F. Rasmussen, B. T. DeVree, Y. Zou, A. C. Kruse, K. Y. Chung, T. S. Kobilka, F. S. Thian, P. S. Chae, E. Pardon, D. Calinski, J. M. Mathiesen, S. T. A. Shah, J. A. Lyons, M. Caffrey, S. H. Gellman, J. Steyaert, G. Skiniotis, W. I. Weis, R. K. Sunahara, B. K. Kobilka, Crystal structure of the β_2 adrenergic receptor–Gs protein complex. *Nature* **477**, 549–555 (2011).
21. Y.-L. Liang, M. Khoshouei, M. Radjainia, Y. Zhang, A. Glukhova, J. Tarrasch, D. M. Thal, S. G. B. Furness, G. Christopoulos, T. Coudrat, R. Danev, W. Baumeister, L. J. Miller, A. Christopoulos, B. K. Kobilka, D. Wootten, G. Skiniotis, P. M. Sexton, Phase-plate cryo-EM structure of a class B GPCR–G-protein complex. *Nature* **546**, 118–123 (2017).
22. Y. Zhang, B. Sun, D. Feng, H. Hu, M. Chu, Q. Qu, J. T. Tarrasch, S. Li, T. Sun Kobilka, B. K. Kobilka, G. Skiniotis, Cryo-EM structure of the activated GLP-1 receptor in complex with a G protein. *Nature* **546**, 248–253 (2017).
23. U. Gether, S. Lin, P. Ghanouni, J. A. Ballesteros, H. Weinstein, B. K. Kobilka, Agonists induce conformational changes in transmembrane domains III and VI of the β_2 adrenoceptor. *EMBO J.* **16**, 6737–6747 (1997).
24. C. Altenbach, K. Yang, D. L. Farrens, Z. T. Farahbakhsh, H. G. Khorana, W. L. Hubbell, Structural features and light-dependent changes in the cytoplasmic interhelical E–F loop region of rhodopsin: A site-directed spin-labeling study. *Biochemistry* **35**, 12470–12478 (1996).
25. C. Hoffmann, G. Gaietta, M. Bünemann, S. R. Adams, S. Oberdorff-Maass, B. Behr, J.-P. Vilardaga, R. Y. Tsien, M. H. Ellisman, M. J. Lohse, A FlAsH-based FRET approach to determine G protein–coupled receptor activation in living cells. *Nat. Methods* **2**, 171–176 (2005).
26. A. D. Stumpf, C. Hoffmann, Optical probes based on G protein-coupled receptors - added work or added value? *Br. J. Pharmacol.* **173**, 255–266 (2016).
27. M. J. Lohse, S. Nuber, C. Hoffmann, Fluorescence/bioluminescence resonance energy transfer techniques to study G-protein-coupled receptor activation and signaling. *Pharmacol. Rev.* **64**, 299–336 (2012).
28. X. Zhang, F. Zhao, Y. Wu, J. Yang, G. W. Han, S. Zhao, A. Ishchenko, L. Ye, X. Lin, K. Ding, V. Dharmarajan, P. R. Griffin, C. Gati, G. Nelson, M. S. Hunter, M. A. Hanson, V. Cherezov, R. C. Stevens, W. Tan, H. Tao, F. Xu, Crystal structure of a multi-domain human smoothened receptor in complex with a super stabilizing ligand. *Nat. Commun.* **8**, 15383 (2017).
29. C. Hoffmann, G. Gaietta, A. Zurn, S. R. Adams, S. Terrillon, M. H. Ellisman, R. Y. Tsien, M. J. Lohse, Fluorescent labeling of tetracysteine-tagged proteins in intact cells. *Nat. Protoc.* **5**, 1666–1677 (2010).
30. K. Bourque, D. Pétrin, R. Sleno, D. Devost, A. Zhang, T. E. Hébert, Distinct conformational dynamics of three G protein-coupled receptors measured using FlAsH-BRET biosensors. *Front. Endocrinol. (Lausanne)* **8**, 61 (2017).
31. C. A. Jost, G. Reither, C. Hoffmann, C. Schultz, Contribution of fluorophores to protein kinase C FRET probe performance. *Chembiochem* **9**, 1379–1384 (2008).
32. A. Ainla, E. T. Jansson, N. Stepanyants, O. Orwar, A. Jesorka, A microfluidic pipette for single-cell pharmacology. *Anal. Chem.* **82**, 4529–4536 (2010).
33. A. Ainla, G. D. M. Jeffries, R. Brune, O. Orwar, A. Jesorka, A multifunctional pipette. *Lab Chip* **12**, 1255–1261 (2012).
34. H.-y. Wang, T. Liu, C. C. Malbon, Structure-function analysis of Frizzleds. *Cell. Signal.* **18**, 934–941 (2006).
35. M. B. C. Kilander, J. Petersen, K. W. Andressen, R. S. Ganji, F. O. Levy, J. Schuster, N. Dahl, V. Bryja, G. Schulte, Disheveled regulates precoupling of heterotrimeric G proteins to Frizzled 6. *FASEB J.* **28**, 2293–2305 (2014).
36. C. Galés, J. J. J. Van Durm, S. Schaak, S. Pontier, Y. Percherancier, M. Audet, H. Paris, M. Bouvier, Probing the activation-promoted structural rearrangements in preassembled receptor–G protein complexes. *Nat. Struct. Mol. Biol.* **13**, 778–786 (2006).
37. C. Galés, R. V. Rebois, M. Hogue, P. Trieu, A. Breit, T. E. Hébert, M. Bouvier, Real-time monitoring of receptor and G-protein interactions in living cells. *Nat. Methods* **2**, 177–184 (2005).
38. M. Bünemann, M. Frank, M. J. Lohse, Gi protein activation in intact cells involves subunit rearrangement rather than dissociation. *Proc. Natl. Acad. Sci. U.S.A.* **100**, 16077–16082 (2003).
39. A. Saulière, M. Bellot, H. Paris, C. Denis, F. Finana, J. T. Hansen, M.-F. Altié, M.-H. Seguelas, A. Pathak, J. L. Hansen, J.-M. Sénard, C. Galés, Deciphering biased-agonism complexity reveals a new active AT_1 receptor entity. *Nat. Chem. Biol.* **8**, 622–630 (2012).
40. M. J. W. Adjobo-Hermans, J. Goedhart, L. van Weeren, S. Nijmeijer, E. M. M. Manders, S. Offermanns, T. W. J. Gadella Jr., Real-time visualization of heterotrimeric G protein Gq activation in living cells. *BMC Biol.* **9**, 32 (2011).
41. J. van Unen, A. D. Stumpf, B. Schmid, N. R. Reinhard, P. L. Hordijk, C. Hoffmann, T. W. J. Gadella Jr., J. Goedhart, A new generation of FRET sensors for robust measurement of $G\alpha_{i1}$, $G\alpha_{i2}$ and $G\alpha_{i3}$ activation kinetics in single cells. *PLOS ONE* **11**, e0146789 (2016).
42. O. Bernatik, K. Šedová, C. Schille, R. S. Ganji, I. Červenka, L. Trantírek, A. Schambony, Z. Zdráhal, V. Bryja, Functional analysis of dishevelled-3 phosphorylation identifies distinct mechanisms driven by casein kinase 1ϵ and frizzled5. *J. Biol. Chem.* **289**, 23520–23533 (2014).
43. S. R. Neves, P. T. Ram, R. Iyengar, G protein pathways. *Science* **296**, 1636–1639 (2002).
44. Y. Namkung, C. LeGouill, S. Kumar, Y. Cao, L. B. Teixeira, V. Lukashova, S. C. Simões, J.-M. Longpré, D. Devost, T. E. Hébert, G. Piñeyro, R. Leduc, C. M. Costa-Neto, M. Bouvier, S. A. Laporte, Functional selectivity profiling of the Angiotensin II type 1 receptor using pathway-wide BRET signaling sensors. *Sci. Signal.* **11**, eaat1631 (2018).
45. E. Alvarez-Curto, A. Inoue, L. Jenkins, S. Z. Raihan, R. Prihandoko, A. B. Tobin, G. Milligan, Targeted elimination of G proteins and arrestins defines their specific contributions to both intensity and duration of G protein-coupled receptor signaling. *J. Biol. Chem.* **291**, 27147–27159 (2016).
46. R. Schröder, N. Janssen, J. Schmidt, A. Kebig, N. Merten, S. Hennen, A. Müller, S. Blättermann, M. Mohr-Andrä, S. Zahn, J. Wenzel, N. J. Smith, J. Gomeza, C. Drewke, G. Milligan, K. Mohr, E. Kostenis, Deconvolution of complex G protein–coupled receptor signaling in live cells using dynamic mass redistribution measurements. *Nat. Biotechnol.* **28**, 943–949 (2010).
47. E. Arthofer, B. Hot, J. Petersen, K. Strakova, S. Jäger, M. Grundmann, E. Kostenis, J. S. Gutkind, G. Schulte, WNT stimulation dissociates a Frizzled 4 inactive-state complex with $G\alpha_{12/13}$. *Mol. Pharmacol.* **90**, 447–459 (2016).
48. B. Hot, J. Valnohova, E. Arthofer, K. Simon, J. Shin, M. Uhlén, E. Kostenis, J. Mulder, G. Schulte, FZD_{10}-$G\alpha_{13}$ signalling axis points to a role of FZD_{10} in CNS angiogenesis. *Cell. Signal.* **32**, 93–103 (2017).
49. K. Qin, C. Dong, G. Wu, N. A. Lambert, Inactive-state preassembly of G_q-coupled receptors and G_q heterotrimers. *Nat. Chem. Biol.* **7**, 740–747 (2011).
50. N. Tüysüz, L. van Bloois, S. van den Brink, H. Begthel, M. M. A. Verstegen, L. J. Cruz, L. Hui, L. J. W. van der Laan, J. de Jonge, R. Vries, E. Braakman, E. Mastrobattista, J. J. Cornelissen, H. Clevers, D. ten Berge, Lipid-mediated Wnt protein stabilization enables serum-free culture of human organ stem cells. *Nat. Commun.* **8**, 14578 (2017).
51. K. Willert, R. Nusse, Wnt proteins. *Cold Spring Harb. Perspect. Biol.* **4**, a007864 (2012).
52. T. Kenakin, Quantifying biological activity in chemical terms: A pharmacology primer to describe drug effect. *ACS Chem. Biol.* **4**, 249–260 (2009).
53. W. M. Oldham, H. E. Hamm, Heterotrimeric G protein activation by G-protein-coupled receptors. *Nat. Rev. Mol. Cell Biol.* **9**, 60–71 (2008).
54. Q. Wan, N. Okashah, A. Inoue, R. Nehmé, B. Carpenter, C. G. Tate, N. A. Lambert, Mini G protein probes for active G protein–coupled receptors (GPCRs) in live cells. *J. Biol. Chem.* **293**, 7466–7473 (2018).
55. T. W. Schwartz, T. M. Frimurer, Full monty of family B GPCRs. *Nat. Chem. Biol.* **13**, 819–821 (2017).
56. E. Alvarez-Curto, J. D. Pediani, G. Milligan, Applications of fluorescence and bioluminescence resonance energy transfer to drug discovery at G protein coupled receptors. *Anal. Bioanal. Chem.* **398**, 167–180 (2010).
57. M. M. Weivoda, M. Ruan, C. M. Hachfeld, L. Pederson, A. Howe, R. A. Davey, J. D. Zajac, Y. Kobayashi, B. O. Williams, J. J. Westendorf, S. Khosla, M. J. Oursler, Wnt signaling

inhibits osteoclast differentiation by activating canonical and noncanonical cAMP/PKA pathways. *J. Bone Miner. Res.* **31**, 65–75 (2016).
58. C. Halleskog, G. Schulte, Pertussis toxin-sensitive heterotrimeric $G_{\alpha i/o}$ proteins mediate WNT/β-catenin and WNT/ERK1/2 signaling in mouse primary microglia stimulated with purified WNT-3A. *Cell. Signal.* **25**, 822–828 (2013).
59. C. Halleskog, J. P. Dijksterhuis, M. B. C. Kilander, J. Becerril-Ortega, J. C. Villaescusa, E. Lindgren, E. Arenas, G. Schulte, Heterotrimeric G protein-dependent WNT-5A signaling to ERK1/2 mediates distinct aspects of microglia proinflammatory transformation. *J. Neuroinflammation* **9**, 111 (2012).
60. V. T. Ramírez, E. Ramos-Fernández, J. P. Henríquez, A. Lorenzo, N. C. Inestrosa, Wnt-5a/Frizzled9 receptor signaling through the $G\alpha_o$-$G\beta\gamma$ complex regulates dendritic spine formation. *J. Biol. Chem.* **291**, 19092–19107 (2016).
61. M. A. Larkin, G. Blackshields, N. P. Brown, R. Chenna, P. A. McGettigan, H. McWilliam, F. Valentin, I. M. Wallace, A. Wilm, R. Lopez, J. D. Thompson, T. J. Gibson, D. G. Higgins, Clustal W and Clustal X version 2.0. *Bioinformatics* **23**, 2947–2948 (2007).
62. B. Webb, A. Sali, Protein structure modeling with *MODELLER*. *Methods Mol. Biol.* **1137**, 1–15 (2014).
63. M.-y. Shen, A. Sali, Statistical potential for assessment and prediction of protein structures. *Protein Sci.* **15**, 2507–2524 (2006).
64. R. Schrage, A.-L. Schmitz, E. Gaffal, S. Annala, S. Kehraus, D. Wenzel, K. M. Büllesbach, T. Bald, A. Inoue, Y. Shinjo, S. Galandrin, N. Shridhar, M. Hesse, M. Grundmann, N. Merten, T. H. Charpentier, M. Martz, A. J. Butcher, T. Slodczyk, S. Armando, M. Effern, Y. Namkung, L. Jenkins, V. Horn, A. Stößel, H. Dargatz, D. Tietze, D. Imhof, C. Galés, C. Drewke, C. E. Müller, M. Hölzel, G. Milligan, A. B. Tobin, J. Gomeza, H. G. Dohlman, J. Sondek, T. K. Harden, M. Bouvier, S. A. Laporte, J. Aoki, B. K. Fleischmann, K. Mohr, G. M. König, T. Tüting, E. Kostenis, The experimental power of FR900359 to study Gq-regulated biological processes. *Nat. Commun.* **6**, 10156 (2015).
65. K. D. Proffitt, B. Madan, Z. Ke, V. Pendharkar, L. Ding, M. A. Lee, R. N. Hannoush, D. M. Virshup, Pharmacological inhibition of the Wnt acyltransferase PORCN prevents growth of WNT-driven mammary cancer. *Cancer Res.* **73**, 502–507 (2013).
66. S. Dorsch, K.-N. Klotz, S. Engelhardt, M. J. Lohse, M. Bünemann, Analysis of receptor oligomerization by FRAP microscopy. *Nat. Methods* **6**, 225–230 (2009).
67. R. D. Phair, S. A. Gorski, T. Misteli, Measurement of dynamic protein binding to chromatin in vivo, using photobleaching microscopy. *Methods Enzymol.* **375**, 393–414 (2004).
68. R. Schröder, J. Schmidt, S. Blättermann, L. Peters, N. Janssen, M. Grundmann, W. Seemann, D. Kaufel, N. Merten, C. Drewke, J. Gomeza, G. Milligan, K. Mohr, E. Kostenis, Applying label-free dynamic mass redistribution technology to frame signaling of G protein–coupled receptors noninvasively in living cells. *Nat. Protoc.* **6**, 1748–1760 (2011).

Acknowledgments: We are grateful to M. M. Maurice for providing the V5-FZD_5 and SNAP-FZD_5 plasmids, M. M. Rasenick for $G\alpha_{i1}$-GFP, and N. A. Lambert for $G\alpha_q$-Venus, Venus-kras, and Venus-Rab5. We thank A. Inoue for providing the $G\alpha_{q/11}$ KO HEK293 cells and for scientific input. **Funding:** The work was supported by grants from Karolinska Institutet (to G.S.), the Swedish Research Council (2015-02899 and 2013-5708 to G.S.), the Swedish Cancer Society (CAN2014/659 and CAN2017/561 to G.S.), Novo Nordisk Fonden (NNF17OC0026940 to G.S.), the Knut and Alice Wallenberg Foundation (KAW2008.0149 to G.S. and 2008.0139 to J.C.), Engkvist's Foundations (to G.S.), the Marie Curie ITN WntsApp (grant no. 608180 to G.S. and C.H.; www.wntsapp.eu), the Swedish Society for Medical Research (SSMF; to S.C.W.), the Science for Life Laboratory (to J.C.), the Deutsche Forschungsgemeinschaft (DFG, German Research Foundation) TRR166: project C2 (to C.H.) and FOR2372 (to E.K. and G.M.K.), and the Canadian Institutes of Health Research (CIHR) (FDN-148431 to M.B. and MOP-74603 to S.A.L.). T.B. is a member of the DFG-funded graduate training school RTG1873. Computational resources were provided by the Swedish National Infrastructure for Computing (SNIC). **Author contributions:** S.C.W., M.C.A.C., T.B., K.S., P.M., and J.C. performed experiments and generated data. C.L.G., Y.N., V.L., M.B., and S.A.L. created and validated BRET probes. G.M.K. provided reagents. S.C.W., M.C.A.C., C.L.G., P.M., J.C., E.K., M.B., G.S., and C.H. planned experiments, analyzed the data, and compiled figures. S.C.W., M.C.A.C., M.B., G.S., and C.H. wrote the paper. **Competing interests:** M.B. is the president of the Scientific Advisory Board of Domain Therapeutics, a company involved in the discovery of drugs targeting GPCRs. All other authors declare that they have no competing interests. **Data and materials availability:** All data needed to evaluate the conclusions in the paper are present in the paper or the Supplementary Materials. All constructs originally described in this study can be obtained for noncommercial purposes on request from the corresponding authors provided suitable material transfer agreements (MTAs) are signed. Patents are held or have been applied for all the BRET biosensors used in the present study. All BRET biosensors can be obtained free from M.B. for noncommercial research purpose upon completion of a regular MTA.

Submitted 29 January 2018
Resubmitted 21 May 2018
Accepted 25 October 2018
Published 4 December 2018
10.1126/scisignal.aar5536

Citation: S. C. Wright, M. C. A. Cañizal, T. Benkel, K. Simon, C. Le Gouill, P. Matricon, Y. Namkung, V. Lukasheva, G. M. König, S. A. Laporte, J. Carlsson, E. Kostenis, M. Bouvier, G. Schulte, C. Hoffmann, FZD_5 is a $G\alpha_q$-coupled receptor that exhibits the functional hallmarks of prototypical GPCRs. *Sci. Signal.* **11**, eaar5536 (2018).

Science Signaling

FZD_5 is a $G\alpha_q$-coupled receptor that exhibits the functional hallmarks of prototypical GPCRs

Shane C. Wright, Maria Consuelo Alonso Cañizal, Tobias Benkel, Katharina Simon, Christian Le Gouill, Pierre Matricon, Yoon Namkung, Viktoria Lukasheva, Gabriele M. König, Stéphane A. Laporte, Jens Carlsson, Evi Kostenis, Michel Bouvier, Gunnar Schulte and Carsten Hoffmann

Sci. Signal. **11** (559), eaar5536.
DOI: 10.1126/scisignal.aar5536

FZD_5 as a prototypical GPCR

Despite exhibiting sequence and structural similarity to other classes of G protein–coupled receptors (GPCRs), class F family members are generally not considered to be prototypical GPCRs. Wright *et al*. found that the class F GPCR FZD_5 exhibited many of the functional characteristics of GPCRs. FZD_5 underwent a conformational change similar to that of conventional GPCRs upon ligand binding. Ligand binding also caused FZD_5 to activate signaling through $G\alpha_q$-containing heterotrimeric G proteins. FZD_5-mediated activation of $G\alpha_q$ elicited the production of second messengers, the activation of kinases, and cellular responses typical of G protein activation by classical GPCRs. These findings suggest that FZD_5 and other class F GPCRs may not differ from prototypical GPCRs as much as was previously thought.